Communications in Nonlinear Science and Numerical Simulation 127 (2023) 107526

Contents lists available at ScienceDirect

Communications in Nonlinear Science and Numerical Simulation

journal homepage: www.elsevier.com/locate/cnsns

Research paper

Interactions of (m, n) and $(m+1, n)$ modes with real eigenvalues: A dynamic transition approach

Taylan Şengül, Burhan Tiryakioglu *

Department of Mathematics, Marmara University, 34722 Istanbul, Turkey

ARTICLE INFO

Article history:
Received 11 May 2023
Received in revised form 7 September 2023
Accepted 8 September 2023
Available online 14 September 2023

Keywords:
Dynamic transition
Center manifold
Rayleigh–Bénard convection
Mode interactions

ABSTRACT

In this work, we consider the multiplicity two dynamic transitions of a broad class of problems. The first main assumption is the existence of two critical eigenmodes of the linear operator which depend on at least two wave indices one of which are consecutive m, $m+1$ and the other identical n. The second main assumption is an orthogonality condition on the nonlinear interactions of the basis vectors of the phase space which is typical in many applications. Under this assumption we obtain a reduced system of ODE's which describe the first dynamic transitions. We make a careful analysis of this reduced system to classify all possible transition behavior. We then apply our main theoretical findings to the 2D Rayleigh–Bénard convection with free-slip boundary conditions and show that this problem displays an S^1 attractor bifurcation.

1. Introduction

In many problems of nonlinear sciences, one has to encounter equations of the form

$$\frac{du}{dt} = \mathcal{L}_\lambda u + \mathcal{G}_\lambda(u). \tag{1}$$

This equation represents a nonlinear dissipative system [1] on a Hilbert space X where $u : [0, \infty) \mapsto X$ is the unknown function and $\lambda \in \mathbb{R}^1$ is a parameter. Here $L_\lambda : X_1 \to X$ is a linear operator where X_1 is another Banach space with compact and dense inclusion $X_1 \subset X$ and $\mathcal{G}_\lambda$ is a nonlinear operator. We assume that the nonlinear operator $\mathcal{G}_\lambda$ consists of higher order terms in u, that is $\mathcal{G}_\lambda(u) = o(\|u\|_{X_\alpha})$ where X_α is an interpolation space with $0 \le \alpha < 1$. This ensures that (1) admits the homogeneous steady state solution

$$u(t) \equiv 0, \qquad \forall t \ge 0. \tag{2}$$

In (1), λ is considered as a driving mechanism, where for small values of λ, the steady state (2) is stable, and there exists a critical value λ_c where this steady state loses its stability as λ crosses λ_c as given by the Principle of Exchange of Stabilities condition below. This phenomenon is known as the first dynamic transition of the steady state solution. In this work, we are interested in analyzing the first dynamic transitions of the steady state solution (2) of (5).

In order to study the first dynamic transition of the steady state, traditionally, a reduced system that captures the dynamics of (1) near the critical value λ_c is obtained. This approach has been widely explored in the literature [2–4].

* Corresponding author.
E-mail addresses: taylan.sengul@marmara.edu.tr (T. Şengül), burhan.tiryakioglu@marmara.edu.tr (B. Tiryakioglu).

https://doi.org/10.1016/j.cnsns.2023.107526
1007-5704/

However, unlike most of the previous work on dynamic transition analysis, we consider general conditions on the problem (1), allowing us to discuss and characterize the dynamic transitions for a family of problems in nonlinear sciences. This direction has been taken in the past in [5–7].

Our main assumptions are the following:

(1) The phase space is spanned by a set of basis vectors $\{e_{m,n,j}\}$ (which we will call as Fourier basis) indexed by three separate indices which we label as the horizontal index m, the vertical index n and the remaining indices j, see Section 2.2 for a detailed explanation.

(2) Denoting the eigenvalues of the linear operator by $\{\beta_i : i \in \mathbb{N}\}$, we assume that there are two first real eigenvalues β_1, β_2 of the linear operator $\mathcal{L}_\lambda$ which become critical at $\lambda = \lambda_c$ while the rest of the spectrum is still stable. That is the following Principle of Exchange of Stabilities condition

$$\beta_1(\lambda), \beta_2(\lambda) \begin{cases} < 0 & \lambda < \lambda_c \\ = 0 & \lambda = \lambda_c \\ > 0 & \lambda > \lambda_c, \end{cases}$$
$$Re\beta_i < 0, \qquad \forall i \geq 3,$$

holds. This means there is a first transition of multiplicity two at $\lambda = \lambda_c$.

(3) The first two critical eigenmodes f_1, f_2 (corresponding to β_1, β_2) and the corresponding adjoint eigenmodes f_1^*, f_2^* are assumed to lie in the space spanned by the Fourier basis with consecutive horizontal indices $m_0 \in \mathbb{Z}$, $m_0 + 1$ and identical non-zero vertical index $n_0 \neq 0$. That is

$$f_1, f_1^* \in H_{m_0,n_0}, \qquad f_2, f_2^* \in H_{m_0+1,n_0},$$

where

$$H_{m,n} = \text{span}\left\{e_{m,n,j} : \forall j \in \mathcal{I}_r\right\},$$

and $\mathcal{I}_r$ denotes the index set of the remaining indices, see Section 2.2.

(4) The nonlinear interactions of the Fourier basis vectors satisfy the following orthogonality relation typically satisfied in applications. For any choice of $\pm$ and any $r = 1, 2$, we assume that

$$\begin{aligned} &\pm i_r \pm j_r \pm k_r \neq 0 \implies \langle \mathcal{G}_2(e_{i_1,i_2,i_3}, e_{j_1,j_2,j_3}), e_{k_1,k_2,k_3}\rangle = 0, \\ &\pm i_r \pm j_r \pm k_r \pm l_r \neq 0 \implies \langle \mathcal{G}_3(e_{i_1,i_2,i_3}, e_{j_1,j_2,j_3}, e_{k_1,k_2,k_3}), e_{l_1,l_2,l_3}\rangle = 0, \end{aligned} \tag{3}$$

where $\mathcal{G}_2$, $\mathcal{G}_3$ are the bilinear and trilinear operators related to the nonlinear operator $\mathcal{G} = \mathcal{G}_\lambda$. This means that, the nonlinear interaction of any number of Fourier basis vectors is zero if the sum of their vertical or horizontal indices does not vanish. This assumption is typical for problems whose nonlinear terms are multi-polynomials of the unknown functions and their gradients.

To illustrate the last assumption, we consider the following example.

Example 1.1. Suppose that $\mathcal{G}(u) = u\frac{\partial u}{\partial x}$, the Fourier basis is given by

$$\left\{e_{i,j,1} = \sin(ix)\sin(jy) : i, j \in \mathbb{N}\right\},$$

and the inner product is defined by $\langle f, g\rangle = \int_0^\pi \int_0^\pi f(x,y)g(x,y)dxdy$. Then $\mathcal{G}_2$ can be chosen as $\mathcal{G}_2(u,v) = uv_x$, $\mathcal{G}_3 \equiv 0$ and the conditions in (3) can easily be seen to hold. In fact the first condition in (3) reads as

$$\int_0^\pi \int_0^\pi \sin(i_1x)\sin(i_2y)j_1\cos(j_1x)\sin(j_2y)\sin(k_1x)\sin(k_2y)dxdy = 0,$$

unless both $\pm i_1 \pm j_1 \pm k_1 = 0$ and $\pm i_2 \pm j_2 \pm k_2 = 0$ which is trivial to check.

Our assumptions are satisfied in a variety of problems, including reaction–diffusion models [6,8–10], binary systems [11–13], and convection phenomena [3,14–18]. When these assumptions hold, we show that the first dynamic transition of (1) leads to a reduced system of the form:

$$\begin{aligned} \frac{dx_1}{dt} &= \beta_1(\lambda)x_1 - x_1(ax_1^2 + bx_2^2) + O(4), \\ \frac{dx_2}{dt} &= \beta_2(\lambda)x_2 - x_2(cx_1^2 + dx_2^2) + O(4). \end{aligned} \tag{4}$$

Here x_1, x_2 are the time-dependent amplitudes of the first two critical modes. β_1, β_2 are the first two critical eigenvalues, and the coefficients a, b, c, d are explicitly calculated and depends on the nonlinear interactions of the critical modes with themselves as well as the remaining stable eigenmodes.

We find that the absence of quadratic terms in (4) is due to the identical vertical wave index (which is n) selection assumption, while the absence of certain cubic terms is a result of the consecutive critical horizontal wave index (which are m and $m + 1$) selection assumption.

In [5], the author derived the reduced dynamical system of (1) without assuming identical vertical wave index selection. As a result, in that paper, the quadratic terms x_1x_2 in the first equation and x_1^2 in the second equation of (4) are present. When those quadratic terms are present, they dictate the dynamics of the reduced system. As a result, it was found that the possible dynamic transition scenarios are greatly reduced. In contrast, in this paper, we assume the identical vertical wave index selection resulting to the absence of quadratic terms which leads to a much richer dynamics of the reduced system.

Our paper provides a complete dynamical transition analysis of (1) by a through analysis of the reduced system (4). We classify all the possible transition scenarios (28 in total) by identifying the phase portraits near the criticality λ_c. Additionally, we demonstrate that the system exhibits an attractor/repeller bifurcation under certain conditions on the coefficients of the reduced system.

We also explore a further assumption in which the linear operator is self-adjoint and the nonlinear operator is both bilinear and energy-preserving. Under these conditions, we show that the first transition is always continuous and accompanied by an S^1 attractor bifurcation.

To demonstrate the practical applicability of our theoretical results, we analyze the 2D Rayleigh–Bénard convection with free-slip boundary conditions. We demonstrate that this problem satisfies all of our main assumptions, allowing us to analyze its first dynamic transition using our theoretical approach.

2. The setting and the main assumptions

We first discuss the main assumptions used in this study.

First of all, we will consider another form of (1) which is the following and which also arises a lot in practical applications.

$$\mathcal{M}_\lambda \frac{du}{dt} = \mathcal{N}_\lambda u + \mathcal{G}_\lambda(u), \tag{5}$$

where $\mathcal{M}_\lambda$ is a linear invertible operator and $\mathcal{N}_\lambda$ is a linear operator. The Eq. (5) can be obtained from (1) by defining $\mathcal{L}_\lambda = \mathcal{M}_\lambda^{-1}\mathcal{N}_\lambda$. When $\mathcal{M}_\lambda = \mathrm{Id}$, the identity operator, then obviously (5) reduces to (1) with $\mathcal{N}_\lambda = \mathcal{L}_\lambda$.

From now on, we suppress the dependence of the operators on λ, so that $\mathcal{M} = \mathcal{M}_\lambda$, $\mathcal{N} = \mathcal{N}_\lambda$ and $\mathcal{G} = \mathcal{G}_\lambda$ to improve readability.

2.1. The assumptions on the spectrum of the linear operator

We will assume that the generalized eigenvalue problem

$$\beta_i \mathcal{M} f_i = \mathcal{N} f_i, \tag{6}$$

related to the linear part of (5) has a countably infinite set of eigenvalues

$$\{\beta_i(\lambda) \in \mathbb{C} : i \in \mathbb{N}\},$$

with a complete set of eigenvectors

$$\{f_i \in X_1, i \in \mathbb{N}\},$$

satisfying the following conditions, known as the Principle of Exchange of Stabilities (PES).

$$\begin{aligned} &\beta_1(\lambda), \beta_2(\lambda) \in \mathbb{R}, \\ &\beta_1(\lambda), \beta_2(\lambda) \begin{cases} < 0 & \lambda < \lambda_c \\ = 0 & \lambda = \lambda_c \\ > 0 & \lambda > \lambda_c, \end{cases} \\ &Re\beta_i < 0, \qquad \forall i \geq 3. \end{aligned} \tag{7}$$

Notice that we require the equality of the first two eigenvalues only for $\lambda = \lambda_c$.

For the reduction procedure we will require a set of adjoint eigenvectors f_j^* determined by the relation

$$\overline{\beta}_i \mathcal{M}^* f_i^* = \mathcal{N}^* f_i^* \tag{8}$$

where $\mathcal{M}^*$ and $\mathcal{N}^*$ are adjoint operators of $\mathcal{M}$ and $\mathcal{N}$ and $\bar{\cdot}$ denotes the complex conjugate. The adjoint eigenvectors have the orthogonality property

$$\langle \mathcal{M} f_j, f_k^* \rangle = \delta_{jk} \langle \mathcal{M} f_j, f_j^* \rangle, \qquad \forall j, k \in \mathbb{N}, \tag{9}$$

with $\langle \cdot, \cdot \rangle$ denoting the inner product in X and δ_{jk} denoting the Kronecker's delta.

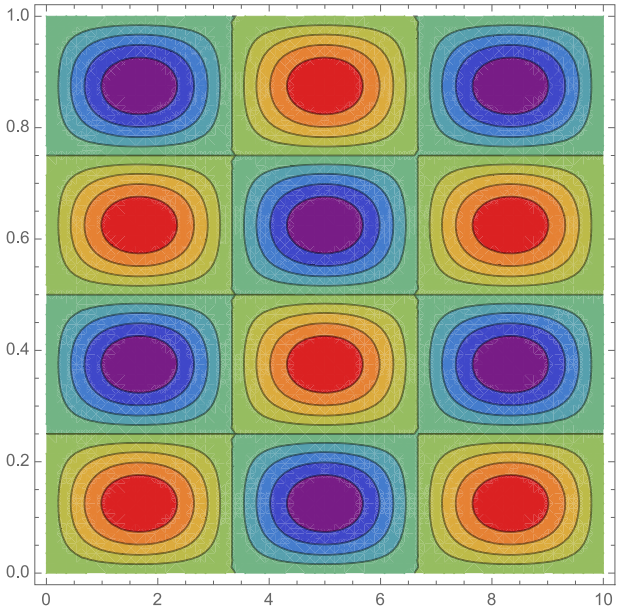

Fig. 1. The spatial structure of the vertical velocity field $\sin\left(\frac{m\pi x}{L}\right)\sin(n\pi z)$ for $m = 3$, $n = 4$, $L = 10$.

2.2. The assumptions on the spatial structure of the eigenmodes

We assume that the phase space X has a basis as follows

$$\{e_{m,n,j} \in X_1 : m \in \mathcal{I}_h, n \in \mathcal{I}_v, j \in \mathcal{I}_r\}, \tag{10}$$

where m denotes the "horizontal" index, n denotes "vertical" index and j denote the rest of the indices. Later, this basis set will be assumed to satisfy some necessary orthogonality conditions with respect to the nonlinear operator, see (18). We remark here the distinction between the basis vectors $e_{m,n,j}$ of the phase space and the eigenmodes of the linear operator f_j which are sometimes identical in applications.

Typically the basis (10) is the Fourier basis of the phase space determined by the boundary conditions of the problem. For the index sets $\mathcal{I}_h$ and $\mathcal{I}_v$, the choice of the set of integers $\mathbb{Z}$, the set of non-negative integers $\mathbb{N}_0$ and the set of positive integers $\mathbb{N}$ are associated with the periodic boundary conditions, Neumann boundary conditions and Dirichlet boundary conditions respectively. The index set $\mathcal{I}_r$ in (10) counts all the distinct Fourier basis vectors with a given horizontal and vertical index. Typically, for problems in two spatial dimensions with n-unknown functions $\mathcal{I}_r = \{n\}$. For problems in spatial dimensions ≥ 3, $\mathcal{I}_r$ is infinite. Thus the spatial domain that is considered is at least two dimensional (horizontal and vertical dimensions).

For example for the 2D Rayleigh–Bénard convection equations with "free-slip" boundary conditions which will be discussed in Section 4, the basis in (10) is given as

$$e_{m,n,1} = \begin{bmatrix} \sin\left(\frac{m\pi x}{L}\right)\sin(n\pi z) \\ 0 \end{bmatrix}, \quad e_{m,n,2} = \begin{bmatrix} 0 \\ \cos\left(\frac{m\pi x}{L}\right)\sin(n\pi z) \end{bmatrix}, \tag{11}$$

where the first component of the vector denotes the stream function and the second component of the vectors denotes the temperature. Here, the spatial variables are $x \in [0, L]$, $z \in [0, 1]$ while $L > 0$ is the aspect ratio of the domain. For this problem,

$$\mathcal{I}_h = \mathbb{N}_0, \qquad \mathcal{I}_v = \mathbb{N}, \qquad \mathcal{I}_r = \{1, 2\}.$$

A typical spatial structure of the stream function field, which is the first component of the first vector in (11), is shown in Fig. 1.

For given $(m, n) \in \mathcal{I}_h \times \mathcal{I}_v$, we define the subspace

$$H_{m,n} = \text{span}\left\{e_{m,n,j} : \forall j \in \mathcal{I}_r\right\}, \tag{12}$$

of the phase space.

One of our main assumption is that the first two critical eigenmodes f_1, f_2 and the adjoint critical eigenmodes f_1^*, f_2^* have the spatial structure given by

$$f_1, f_1^* \in H_{m_0,n_0}, \qquad f_2, f_2^* \in H_{m_0+1,n_0}, \tag{13}$$

while the rest of the eigenmodes are orthogonal to them, that is

$$f_k, f_k^* \in (H_{m_0,n_0} \oplus H_{m_0+1,n_0})^{\perp}, \qquad \forall k \geq 3, \tag{14}$$

the horizontal index is an integer

$$m_0 \in \mathbb{Z}, \tag{15}$$

and the vertical index is non-zero

$$n_0 \neq 0. \tag{16}$$

That is the first two critical eigenmodes have consecutive horizontal indices, and identical non-zero vertical index.

For example, as we shall see later, for the Rayleigh–Bénard convection problem, the critical horizontal index is $m_0 \in \mathbb{N}_0$ and the critical vertical index is always $n_0 = 1$ and by (13), we mean

$$f_1 = c_{1,1} e_{m_0,1,1} + c_{1,2} e_{m_0,1,2},$$
$$f_2 = c_{2,1} e_{m_0+1,1,1} + c_{2,2} e_{m_0+1,1,2},$$

where $c_{i,j}$, $i, j = 1, 2$ are scalars.

2.3. The assumption of orthogonality of the nonlinear interactions of the basis vectors

We consider the following expansion of $\mathcal{G}$.

$$\mathcal{G}(u) = \mathcal{G}_2(u, u) + \mathcal{G}_3(u, u, u) + \cdots \tag{17}$$

Here $\mathcal{G}_2$ is the bilinear and $\mathcal{G}_3$ is the trilinear operator of the expansion of $\mathcal{G}$. We recall that $\mathcal{G}$ does not contain linear terms and the rest of the expansion consists of higher order terms which will not play a role in the subsequent analysis.

Remark 2.1. There are infinitely many ways of choosing operators $\mathcal{G}_2$, $\mathcal{G}_3$. For example, if $\mathcal{G}(u) = uu_x$ then $\mathcal{G}_2$ can be chosen as

$$\mathcal{G}_2(u, v) = cuv_x + (1 - c)vu_x,$$

for each $c \in \mathbb{R}$. The results in this paper are independent of the choice of $\mathcal{G}_2$, $\mathcal{G}_3$. In fact one can always choose these operators to be symmetric. For the above example this is satisfied for $c = 1/2$.

The main assumption on the nonlinear operator is the following orthogonality conditions on the bilinear $\mathcal{G}_2$ and trilinear $\mathcal{G}_3$ interactions of the Fourier basis vectors $e_{m,n,j}$. We assume that for any choice of $\pm$ and any $r = 1, 2$, we have

$$\begin{aligned} &\pm i_r \pm j_r \pm k_r \neq 0 \implies \langle \mathcal{G}_2(e_{i_1,i_2,i_3}, e_{j_1,j_2,j_3}), e_{k_1,k_2,k_3} \rangle = 0, \\ &\pm i_r \pm j_r \pm k_r \pm l_r \neq 0 \implies \langle \mathcal{G}_3(e_{i_1,i_2,i_3}, e_{j_1,j_2,j_3}, e_{k_1,k_2,k_3}), e_{l_1,l_2,l_3} \rangle = 0, \end{aligned} \tag{18}$$

where $i_1, j_1, k_1, l_1 \in \mathcal{I}_h$, $i_2, j_2, k_2, l_2 \in \mathcal{I}_v$, $i_3, j_3, k_3, l_3 \in \mathcal{I}_r$.

Basically, the condition (18) means that the nonlinear interaction of a number of Fourier basis vectors is zero if the sum of their vertical or horizontal indices does not vanish.

For ease of notation, for $i, j, k, l \in \mathbb{N}$ we will denote the bilinear and trilinear interactions of the eigenmodes by

$$\begin{aligned} g_2(i, j, k) &= \frac{1}{\langle \mathcal{M} f_k, f_k^* \rangle} \langle \mathcal{G}_2(f_i, f_j), f_k^* \rangle, \\ g_2^s(i, j, k) &= g_2(i, j, k) + g_2(j, i, k). \end{aligned} \tag{19}$$

Similarly for the trilinear operator,

$$\begin{aligned} g_3(i, j, k, l) &= \frac{1}{\langle \mathcal{M} f_l, f_l^* \rangle} \langle \mathcal{G}_3(f_i, f_j, f_k), f_l^* \rangle, \\ g_3^s(i, j, k, l) &= \sum_{\sigma} g_3(\sigma(i, j, k), l), \end{aligned} \tag{20}$$

where the summation is over all permutations σ of the triple (i, j, k).

Now we list some consequences (Lemmas 2.1 and 2.2) of the main assumptions using the notation above. These will be used in the reduction procedure.

Lemma 2.1.

$$g_2(i, j, k) = g_2^s(i, j, k) = 0, \qquad \forall i, j, k \in \{1, 2\}. \tag{21}$$

Proof. The assumption (13) and the first condition in (18) imply that

$$\langle \mathcal{G}_2(f_i, f_j), f_k^* \rangle = 0, \qquad \forall i, j, k = 1, 2, \tag{22}$$

since for some $c \in \mathbb{R}$

$$\langle \mathcal{G}_2(f_i, f_j), f_k^* \rangle = c \langle \mathcal{G}_2(e_{\cdot, n_0, \cdot}, e_{\cdot, n_0, \cdot}), e_{\cdot, n_0, \cdot} \rangle,$$

which is zero since $\pm n_0 \pm n_0 \pm n_0 \neq 0$, thanks to the assumption that $n_0 \neq 0$, see (16).

Now (22) implies the result.

As we shall later see, the above lemma is the reason for the vanishing of the quadratic terms in the reduced system (25). On the other hand, and again as we shall later see, the below lemma gives rise to the structure of the cubic terms of the reduced system.

Lemma 2.2.

If $i + j + k + l$ is odd then $g_3(i, j, k, l) = 0, \qquad \forall i, j, k, l \in \{1, 2\},$ (23)

and in particular,

$$g_3^s(1, 1, 2, 1) = g_3^s(2, 2, 2, 1) = g_3^s(1, 2, 2, 2) = g_3^s(1, 1, 1, 2) = 0. \tag{24}$$

Proof. For $i, j, k, l \in \mathbb{Z}$, we define the following sets

$$S(i, j, k, l) = \{\pm i \pm j \pm k \pm l : \text{for any choice of } \pm\}.$$

Since by (15), $m_0 \in \mathbb{Z}$, we have

$$0 \notin S(m_0, m_0 + 1, m_0 + 1, m_0 + 1) = \{\pm 1, \pm(1 + 2m_0), \pm(3 + 2m_0), \pm(3 + 4m_0)\},$$
$$0 \notin S(m_0, m_0, m_0, m_0 + 1) = \{\pm 1, \pm(1 + 2m_0), \pm(2m_0 - 1), \pm(1 + 4m_0)\}.$$

The result follows from the second condition in (18).

Remark 2.2. Since

$$0 \in S(m_0, m_0, m_0, m_0),$$
$$0 \in S(m_0, m_0, m_0 + 1, m_0 + 1),$$
$$0 \in S(m_0 + 1, m_0 + 1, m_0 + 1, m_0 + 1).$$

the cubic interaction terms

$$g_3(1, 1, 1, 1), \qquad g_3^s(1, 2, 2, 1), \qquad g_3^s(1, 1, 2, 2), \qquad g_3(2, 2, 2, 2)$$

are possibly non-zero, see (26).

3. Main results

In this section, we present our main findings. Firstly, we note that the PES condition outlined in (7) implies that the system undergoes a transition from the trivial equilibrium solution (2) as the parameter λ crosses the critical value λ_c. We begin by introducing the reduced system of ordinary differential equations that capture the dynamics of the main Eq. (5) near λ_c. We then analyze the existence and stability of the steady states of this system and classify all possible multiplicity two dynamic transitions based on the coefficients of the reduced system. A total of 68 distinct phase portraits near $\lambda = \lambda_c$ are identified. We classify the phase portraits that occur on $\lambda > \lambda_c$ according to the dynamic transition classification given in [3] and present the results in Theorem 3.1.

Subsequently, we investigate the S^1 attractor/repeller bifurcations of the system and identify conditions on the coefficients of the reduced system that guarantee such bifurcations, as detailed in Theorem 3.2. Finally, we examine a special case where the linear operator is self-adjoint, the nonlinear term is bilinear, and bilinearity can be chosen as energy-preserving, which are typical assumptions for the 2D Navier–Stokes equations. Under these conditions, we demonstrate that the system undergoes a continuous transition accompanied by a S^1 attractor bifurcation.

3.1. The reduced system of ODE's

Let us denote the solution of (5) as

$$u(t) = \sum_{n=1}^{\infty} x_n(t) f_n,$$

where f_n are the eigenmodes of the linear operator.

In Section 5.1 we will show that the main Eq. (5) reduces to the following system of ODE's for sufficiently small initial conditions and near $\lambda = \lambda_c$.

$$\begin{aligned} \frac{dx_1}{dt} &= \beta_1(\lambda)x_1 - x_1(ax_1^2 + bx_2^2) + O(4), \\ \frac{dx_2}{dt} &= \beta_2(\lambda)x_2 - x_2(cx_1^2 + dx_2^2) + O(4). \end{aligned} \tag{25}$$

Here x_1 and x_2 are the time dependent amplitudes of the critical eigenmodes f_1, f_2. The coefficients of the reduced system (25) are given by

$$\begin{aligned} a &= -g_3(1,1,1,1) + \sum_{k=3}^{\infty} \frac{1}{\beta_k} g_2(1,1,k) g_2^s(1,k,1), \\ b &= -g_3^s(1,2,2,1) + \sum_{k=3}^{\infty} \frac{1}{\beta_k} \left(g_2^s(1,2,k) g_2^s(2,k,1) + g_2(2,2,k) g_2^s(1,k,1) \right), \\ c &= -g_3^s(1,1,2,2) + \sum_{k=3}^{\infty} \frac{1}{\beta_k} \left(g_2^s(1,2,k) g_2^s(1,k,2) + g_2(1,1,k) g_2^s(2,k,2) \right), \\ d &= -g_3(2,2,2,2) + \sum_{k=3}^{\infty} \frac{1}{\beta_k} g_2(2,2,k) g_2^s(2,k,2), \end{aligned} \tag{26}$$

where the notations used above are given in (19) and (20).

3.2. The existence and the stability of the steady states

In Section 5.2, we analyze the reduced system (25) and find the possible equilibria and determine their stability near the critical parameter $\lambda = \lambda_c$.

The possible steady states of the main Eq. (5) near the critical parameter λ_c are as follows.

1. The trivial steady state is

   $$TS = 0,$$

   which always exists.
2. The four possible "pure" steady states $PS_1^{\pm}$ and $PS_2^{\pm}$ which are

   $$PS_1^{\pm} = \pm\sqrt{\frac{\beta_1}{a}} f_1 + o(|\beta_1|^{1/2}), \qquad PS_2^{\pm} = \pm\sqrt{\frac{\beta_2}{d}} f_2 + o(|\beta_2|^{1/2}).$$

3. The four possible "mixed" steady states $MS_i^{\pm}$ $(i = 1, 2)$ which are

   $$MS_i^{\pm} = (-1)^i \tilde{x}_1 f_1 + (-1)^j \tilde{x}_2 f_2 + o(|\beta_1|^{1/2} + |\beta_2|^{1/2}), \qquad i = 1, 2,$$

   where

   $$\tilde{x}_1^2 = \frac{M_1}{M_3}, \qquad \tilde{x}_2^2 = \frac{M_2}{M_3},$$

and

$$\begin{aligned} M_1 &= d\beta_1 - b\beta_2, \\ M_2 &= -c\beta_1 + a\beta_2, \\ M_3 &= ad - bc. \end{aligned} \tag{27}$$

In Table 1, the existence and the stability conditions of the steady states of (5) are given. The analysis of Table 1 gives a total of 68 phase portraits in a neighborhood of $\lambda = \lambda_c$ which are summarized in Table 2. These phase portraits give a complete characterization of the dynamical behavior near the criticality $\lambda = \lambda_c$.

In Table 2, we allow β_1, β_2 to have different signs which may seem contradictory to the PES condition (7). The reason for this is that in applications, usually the critical control parameter λ_c at which a multiplicity two transition takes place, depends on the fine-tuning of the other system parameters. This will be apparent in the study of the Rayleigh–Bénard convection problem in Section 4. For the Rayleigh–Bénard convection problem, $\lambda_c = R_c$ which is the critical Rayleigh number at which a multiplicity two transition occurs exists only at critical values L_c of the aspect ratio L, see Fig. 2 and the discussion below it. When L is near L_c but not equal to it, the PES condition (7) is no longer valid as stated, and the first transition is due to the critical crossing of a single eigenvalue. In Table 2, our aim is to classify all the transitions near such a multiplicity two transition point $(\lambda, L) = (R_c, L_c)$. For that reason we allow β_1, β_2 to have different signs in Table 2.

Table 1
The existence and stability of the fixed points of (5).

Fixed point	Existence condition	Stability conditions
TS	Always exists	$\beta_1 < 0$ and $\beta_2 < 0$
$PS_1^{\pm}$	$\beta_1 a > 0$	$\beta_1 > 0$ and $M_2 a < 0$
$PS_2^{\pm}$	$\beta_2 d > 0$	$\beta_2 > 0$ and $M_1 d < 0$
$MS_i^{\pm}$	M_1, M_2, M_3 have same sign	$aM_1 + dM_2 > 0$ and $M_1, M_2, M_3 > 0$

Table 2
The existence and stability of steady states in all the possible phase portraits of (5) near $(u, \lambda) = (0, \lambda_c)$. Here dne=does not exist, sad=saddle, sn=stable node, un=unstable node.

	$\beta_1 > 0$ and $\beta_2 > 0$																
	①	②	③	④	⑤	⑥	⑦	⑧	⑨	⑩	⑪	⑫	⑬	⑭	⑮	⑯	⑰
TS	un	un	un	un	un	un	un	un	un	un	un	un	un	un	un	un	un
PS_1	sad	sn	sn	sad	sad	sad	sad	dne	dne	dne	dne	sn	dne	sad	sn	dne	dne
PS_2	sn	sn	sad	sad	dne	sad	dne	sad	sad	dne	dne	dne	sn	dne	dne	sn	sad
MS	dne	sad	dne	sn	dne	dne	un	dne	un	dne	sad	sad	sad	sn	dne	dne	sn
	$\beta_1 < 0$ and $\beta_2 > 0$																
	⑱	⑲	⑳	㉑	㉒	㉓	㉔	㉕	㉖	㉗	㉘	㉙	㉚	㉛	㉜	㉝	㉞
TS	sad	sad	sad	sad	sad	sad	sad	sad	sad	sad	sad	sad	sad	sad	sad	sad	sad
PS_1	dne	dne	dne	dne	dne	dne	dne	sad	un	un	sad	un	sad	un	un	sad	sad
PS_2	sn	dne	sad	sn	sad	dne	dne	sn	sn	sn	dne	dne	dne	dne	sad	sad	sad
MS	dne	dne	sn	sad	dne	un	sn	dne	sad	dne	un	dne	dne	sad	dne	sn	un
	$\beta_1 > 0$ and $\beta_2 < 0$																
	㉟	㊱	㊲	㊳	㊴	㊵	㊶	㊷	㊸	㊹	㊺	㊻	㊼	㊽	㊾	㊿	(51)
TS	sad	sad	sad	sad	sad	sad	sad	sad	sad	sad	sad	sad	sad	sad	sad	sad	sad
PS_1	sn	sad	sn	sn	sad	sad	sad	sad	sn	sn	dne	dne	dne	dne	dne	dne	dne
PS_2	dne	dne	un	sad	un	sad	sad	dne	dne	un	dne	dne	dne	un	sad	un	sad
MS	dne	sn	sad	dne	dne	un	sn	dne	sad	dne	dne	sn	un	dne	un	sad	dne
	$\beta_1 < 0$ and $\beta_2 < 0$																
	(52)	(53)	(54)	(55)	(56)	(57)	(58)	(59)	(60)	(61)	(62)	(63)	(64)	(65)	(66)	(67)	(68)
TS	sn	sn	sn	sn	sn	sn	sn	sn	sn	sn	sn	sn	sn	sn	sn	sn	sn
PS_1	dne	dne	dne	dne	dne	dne	dne	sad	un	sad	un	sad	sad	sad	un	sad	un
PS_2	dne	sad	dne	un	sad	sad	un	dne	dne	dne	dne	dne	sad	sad	sad	un	un
MS	dne	dne	sad	dne	un	sn	sad	dne	sad	un	dne	sn	un	dne	dne	dne	sad

3.3. The classification of the dynamic transitions

In this subsection, we present a classification of the multiplicity two transitions of the system (5) when both critical eigenvalues β_1 and β_2 become positive. We use the classification scheme given in [3], which defines three types of transitions: Type-I (continuous), Type-II (jump), and Type-III (mixed). The exact definitions of these types can be found in [3], but in general, Type-I transitions lead to solutions that converge to a local attractor, Type-II transitions result in solutions that leave the neighborhood of the origin, and Type-III transitions exhibit a mixture of Type-I and Type-II behavior.

We display all possible transition scenarios of the system (5) near λ_c in Figs. 4–11, which correspond to 28 different scenarios near the critical λ value. The second and fourth quadrants in these figures are related to simple multiplicity transitions when only one of the first two eigenvalues β_1 or β_2 becomes unstable. The third quadrant is the pre-transition region where both critical eigenvalues are negative, and the trivial steady state $u \equiv 0$ is stable. The first quadrant is the region where both eigenvalues are unstable, and a multiplicity two transition takes place.

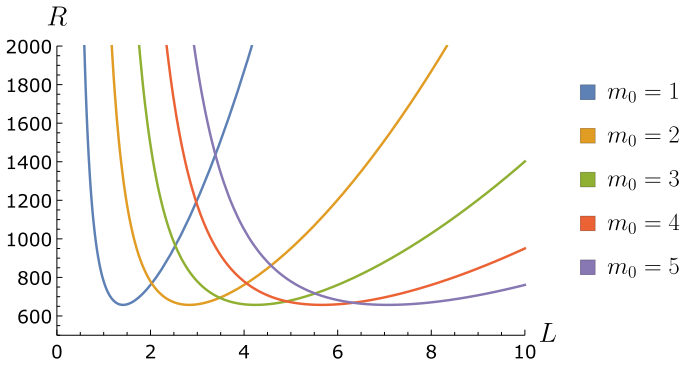

Fig. 2. The marginal stability curves, where $\beta_{m_0,1,1} = 0$.

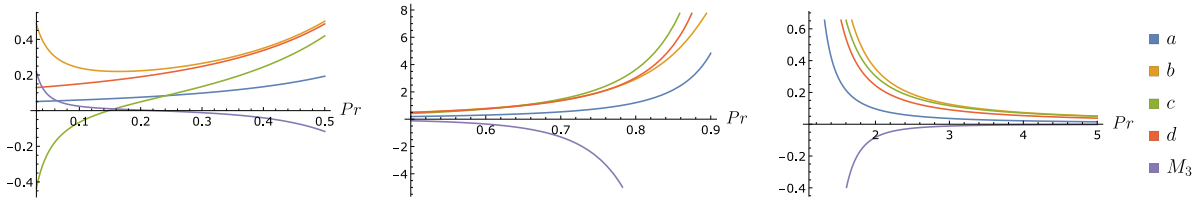

(A) $0 < Pr < 0.5$. (B) $0.5 < Pr < 0.9$. (C) $1 < Pr < 5$.

Fig. 3. The coefficients a, b, c, d and $M_3 = ad - bc$ for $m_0 = 1$ versus the Prandtl number Pr.

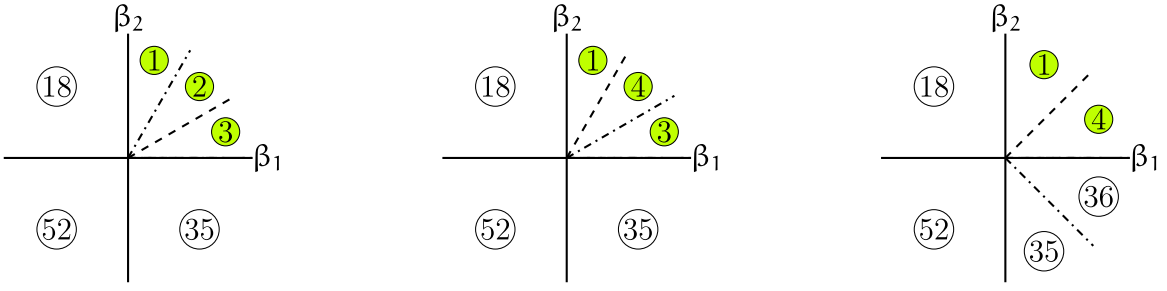

(A) $c > 0$, $M_3 < 0$. (B) $c > 0$, $M_3 > 0$. (C) $c < 0$, $M_3 > 0$.

Fig. 4. Transition scenarios for $a > 0, b > 0, d > 0$. The case $c > 0$ correspond to the attractor bifurcation theorem, Theorem 3.2.

Due to the large number (68 in total) of possible phase portraits, we only show those corresponding to multiplicity two transitions when both eigenvalues are critical in Figs. 12–18. We present the classification of these transitions in the following theorem.

Theorem 3.1. *The system exhibits multiplicity two transitions on $\lambda > \lambda_c$ where $\beta_1 > 0$, $\beta_2 > 0$ by the principle of exchange of stabilities condition (7). Depending on the reduced equation coefficients a, b, c, d and the first two eigenvalues β_1, β_2, the relation between possible phase portraits near $(u, \lambda) = (0, \lambda_c)$ and $\lambda > \lambda_c$ and the corresponding dynamic transitions are as follows.*

1. *The phase portraits (1), (2), (3), (4) as shown in Fig. 12 and also in Fig. 14 correspond to **Type-I** transition.*
2. *The phase portraits (5), (6), (7), (8), (9), (10), (11) as shown in Fig. 16 correspond to **Type-II** transition.*
3. *The phase portraits (12), (13) as shown in Fig. 17 correspond to **Type-III** transition.*

Remark 3.1 (*Ambiguous dynamic transitions*)**.** In the case of phase portraits (14), (15), (16), and (17), which are also observed when both β_1 and β_2 are positive as depicted in Fig. 18, their transition types are ambiguous and cannot be determined

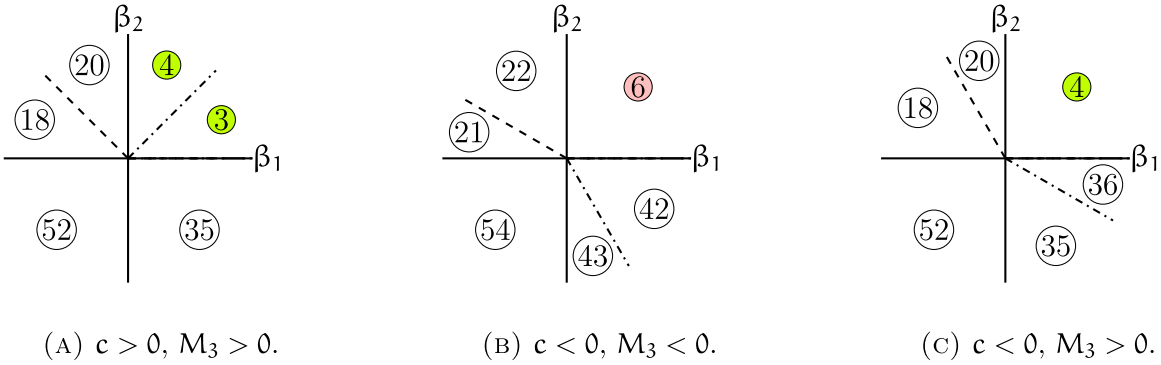

(A) $c > 0,\ M_3 > 0.$ (B) $c < 0,\ M_3 < 0.$ (C) $c < 0,\ M_3 > 0.$

Fig. 5. Transition scenarios for $a > 0, b < 0, d > 0$.

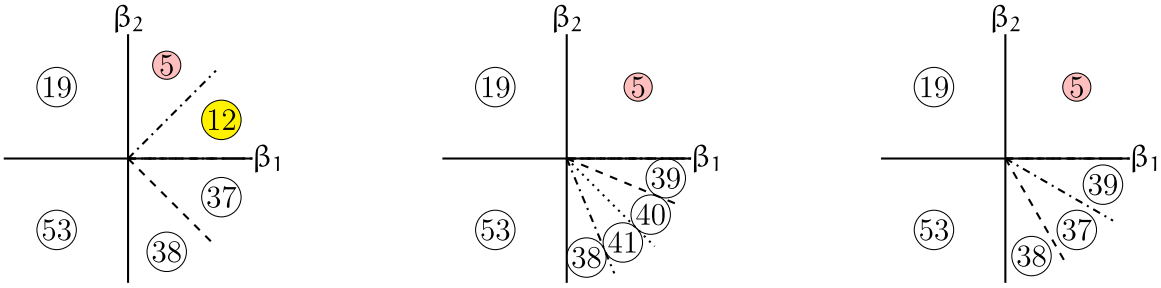

(A) $c > 0,\ M_3 < 0.$ (B) $c < 0,\ M_3 > 0.$ (C) $c < 0,\ M_3 < 0.$

Fig. 6. Transition scenarios for $a > 0, b > 0, d < 0$.

from the reduced system (25). In these instances, the orbits starting from a sector of initial conditions moves out of the neighborhood and then converges to the local steady states in the reduced system. However, the fact that orbits leave the local neighborhood (even though they later re-enter this neighborhood) implies that the reduced equation is not sufficient to determine the trajectories of these initial conditions. To address this ambiguity, we suggest that considering a higher-order approximation of the reduced system could be a viable solution.

3.4. S^1 attractor bifurcation theorem

In this subsection, we investigate the S^1 attractor (resp. repeller) bifurcation phenomena on $\lambda > \lambda_c$ (resp. on $\lambda < \lambda_c$). We recall that an S^1 bifurcated attractor is an invariant attractor Ω_λ which is homeomorphic to S^1 such that

$$\lim_{\lambda \to \lambda_c^+} \operatorname{dist}(\Omega_\lambda, 0) = \lim_{\lambda \to \lambda_c^+} \max_{x \in \Omega_\lambda} |x| = 0.$$

A bifurcated repeller can be defined similarly.

We first give two statements:

1. **Statement 1**: There is an S^1 attractor bifurcation on $\beta_1 > 0$, $\beta_2 > 0$ and the transition is of Type-I. Moreover this attractor consists of either 4 or 8 steady states half of which are saddles and the rest are stable nodes, and the heteroclinic orbits between them.
2. **Statement 2**: There is an S^1 repeller bifurcation on $\beta_1 < 0$, $\beta_2 < 0$ and the transition is of Type-II.

The next theorem gives certain conditions under which these statements hold true.

Theorem 3.2. *Let*

$$\Delta = (b + c)^2 - 4ad,$$

where a, b, c, d are the coefficients of the reduced system and are given by (26).

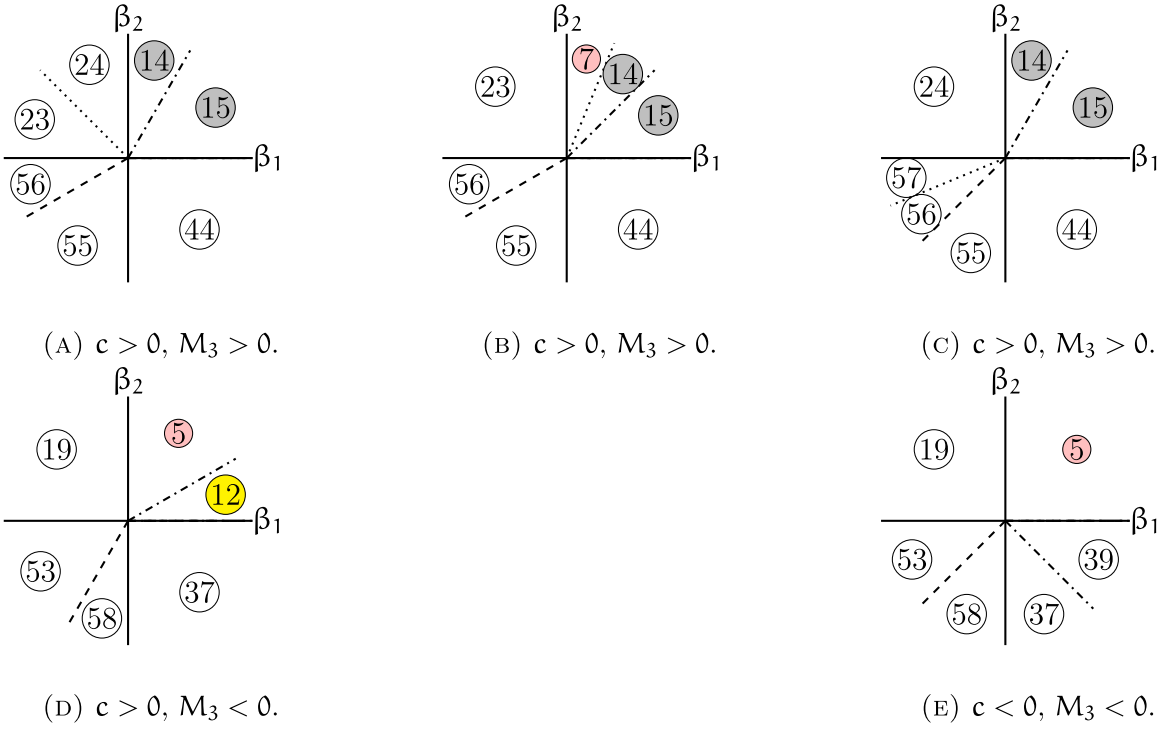

Fig. 7. Transition scenarios for $a > 0, b < 0, d < 0$. The Figs. 7(a), 7(b), 7(c) differ by the choice of $aM_1 + dM_2$ shown by dotted line.

Under each of the following conditions ***Statement 1*** *holds:*

(1) $\Delta < 0$ *and* $a > 0$,
(2) $a > 0$, $b + c > 0$ *and* $d > 0$,
(3) $a > 0$, $d > 0$ *and* $b + c > -2\sqrt{ad}$.

Under each of the following conditions ***Statement 2*** *holds:*

(4) $\Delta < 0$ *and* $a < 0$,
(5) $a < 0$, $b + c < 0$ *and* $d < 0$,
(6) $a < 0$, $d < 0$ *and* $b + c < 2\sqrt{ad}$.

Proof. We only prove (1), (2), (3), the proofs of (4), (5), (6) are identical. By taking the product of the reduced system (25) by (x_1, x_2) and adding, we obtain

$$\frac{d}{2dt}(x_1^2 + x_2^2) = \beta_1 x_1^2 + \beta_2 x_2^2 - K(x_1, x_2) + O(5), \tag{28}$$

where

$$K(x_1, x_2) := ax_1^4 + (b + c)x_1^2 x_2^2 + dx_2^4. \tag{29}$$

If (1) holds then $\Delta < 0$ and $a > 0$ and there exists $\epsilon > 0$ such that

$$K(x_1, x_2) \geq \epsilon \|x\|^4, \qquad \forall (x_1, x_2) \in \mathbb{R}^2, \tag{30}$$

where $\|x\|^2 = x_1^2 + x_2^2$. To see this, let

$$K_\epsilon(x, y) = K(x_1, x_2) - \epsilon\|x\|^4 = (a - \epsilon)x_1^4 + (b + c - 2\epsilon)x_1^2 x_2^2 + (d - \epsilon)x_2^4.$$

Then for sufficiently small $\epsilon > 0$ we have $(a - \epsilon) > 0$ and

$$\Delta_\epsilon = (b + c - 2\epsilon)^2 - 4(a - \epsilon)(d - \epsilon) = \Delta + O(\epsilon) < 0.$$

Thus

$$K_\epsilon(x_1, x_2) \leq 0, \qquad \forall (x_1, x_2) \in \mathbb{R}^2.$$

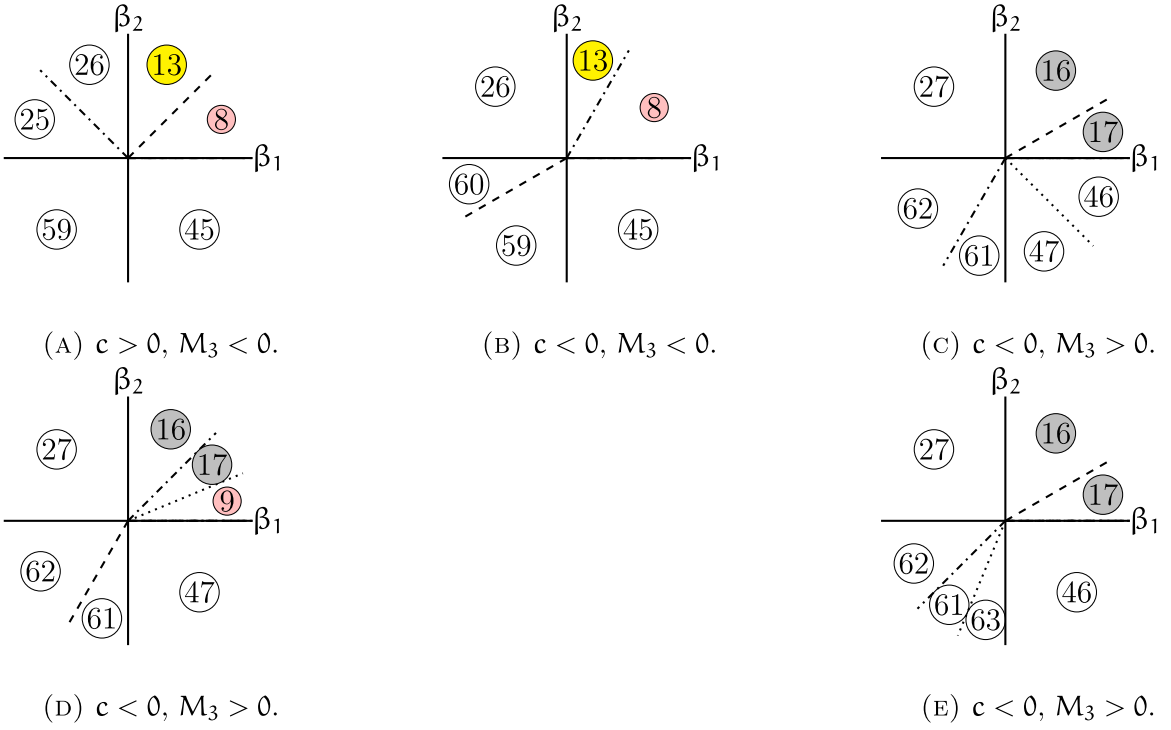

Fig. 8. Transition scenarios for $a < 0, b > 0, d > 0$. The Figs. 8(c), 8(d), 8(e) differ by the choice of $aM_1 + dM_2$ shown by dotted line.

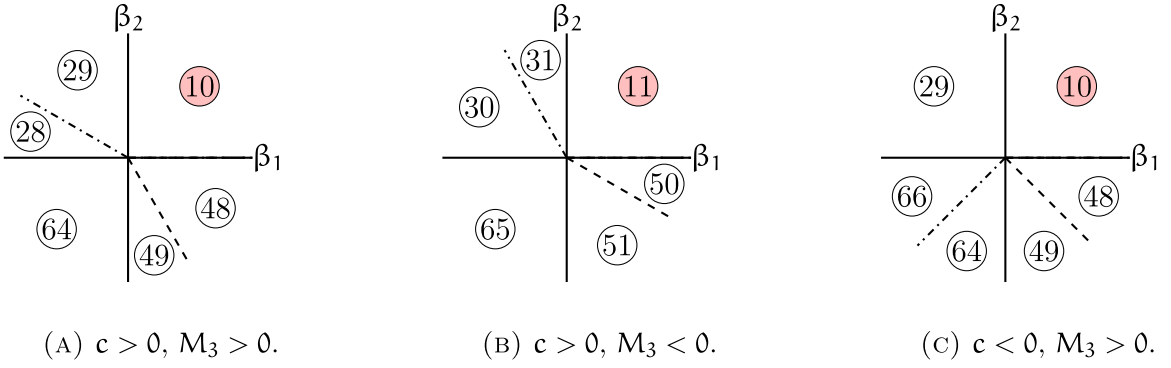

Fig. 9. $a < 0, b > 0, d < 0$.

Now by choosing $\beta = \max\{\beta_1, \beta_2\} > 0$, (28) becomes

$$\frac{d}{2dt}\|x\|^2 \leq 2\beta\|x\|^2 - \epsilon\|x\|^4 + O(5).$$

Now by the application of the attractor bifurcation theorem (Theorem 5.10 in [4]) Statement 1 follows.

The proof in the case (2) is similar and thus omitted. For the proof in the case (3), we note that if $b + c > 0$ then this is the case (2) and the proof is already finished. Otherwise

$$\Delta = (b + c)^2 - 4ad < 0,$$

which is exactly the case (1) and the proof is once again finished.

Remark 3.2. The transition scenarios for the case $a > 0$, $b + c > 0$, $d > 0$ are shown in Fig. 4. By Theorem 3.2, we know that an S^1 attractor bifurcation (Statement 1) occurs in this case. Hence the phase portraits ①, ②, ③ and ④ must correspond to an S^1 attractor bifurcation. This is evident from their schematic phase portraits, see Fig. 12 and also the numerical phase portraits Fig. 14.

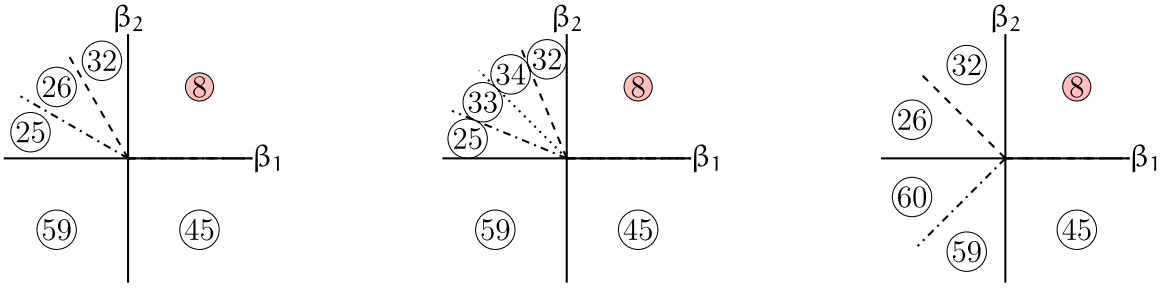

(A) $c > 0$, $M_3 < 0$. (B) $c > 0$, $M_3 > 0$. (C) $c < 0$, $M_3 < 0$.

Fig. 10. Transition scenarios for $a < 0, b < 0, d > 0$.

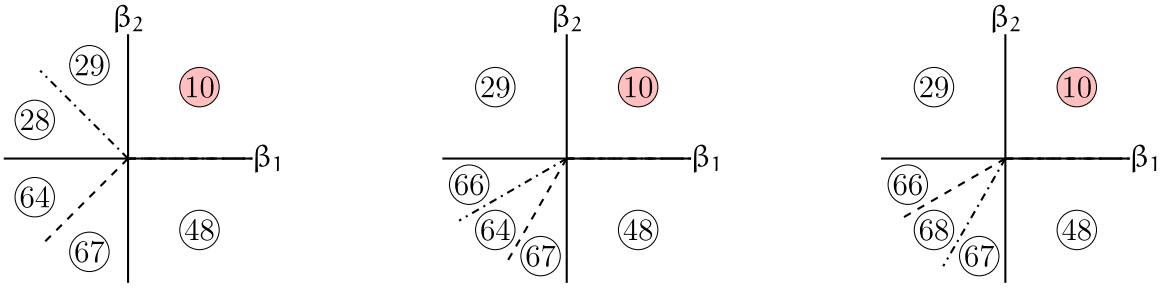

(A) $c > 0$, $M_3 > 0$. (B) $c < 0$, $M_3 > 0$. (C) $c < 0$, $M_3 < 0$.

Fig. 11. Transition scenarios for $a < 0, b < 0, d < 0$. The case $c < 0$ correspond to the attractor bifurcation theorem, Theorem 3.2.

Similarly the transition scenarios for the case $a < 0$, $b + c < 0$, $d < 0$ are shown in Fig. 11. By Theorem 3.2, we know that an S^1 repeller bifurcation (Statement 2) occurs in this case. Hence the phase portraits (64), (66), (67) and (68) which occur on $\beta_1 < 0$, $\beta_2 < 0$ must correspond to an S^1 repeller. These phase portraits are shown schematically in Fig. 13 and numerically in Fig. 15.

Remark 3.3. In the proof above, for $\Delta \geq 0$ case, we write

$$K(x_1, x_2) = a(x_1^2 - \lambda_- x_2^2)(x_1^2 - \lambda_+ x_2^2),$$

where

$$\lambda_\pm = \frac{-(b+c) \pm \sqrt{\Delta}}{2a}.$$

Basic analysis shows that

$$\lambda_\pm < 0 \iff \lambda_-\lambda_+ = d/a > 0 \text{ and } -(\lambda_- + \lambda_+) = \frac{b+c}{a} > 0,$$

and under the condition where both $\lambda_\pm$ are negative, a, $b + c$ and d must be of the same sign and depending on the sign of a exactly one of the conditions (2) or (5) in Theorem 3.2 must hold true.

If exactly one, or both of $\lambda_\pm$ is/are positive, then the situation is more complicated which we plan to address in a future study.

3.5. Self-adjoint linear operator with energy preserving bilinear nonlinearity

When the linear operator is self-adjoint, the nonlinearity is bilinear and energy preserving which is the typical case for the Navier Stokes equations, we show that the transition is always Type-I and there is an attractor bifurcation on $\lambda > \lambda_c$.

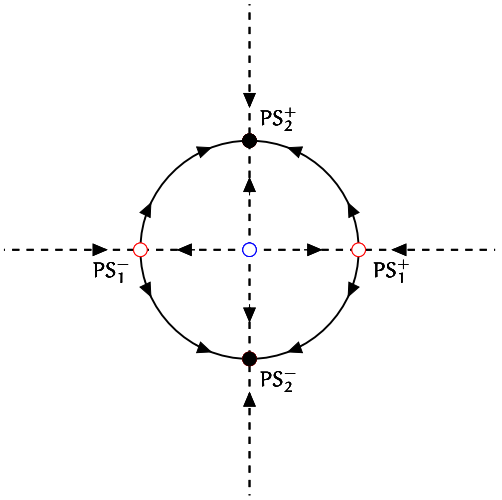

(A) The bifurcated attractor for ①. $PS_1^{\pm}$ saddle, $PS_2^{\pm}$ stable and $MS_{12}^{\pm}$ does not exist.

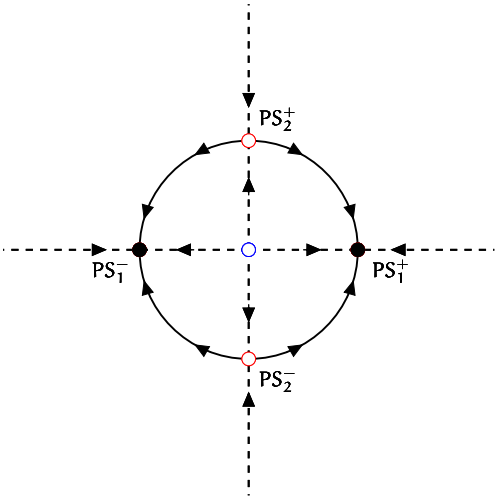

(B) The bifurcated attractor for ③. $PS_1^{\pm}$ stable, $PS_2^{\pm}$ saddle and $MS_{12}^{\pm}$ does not exist.

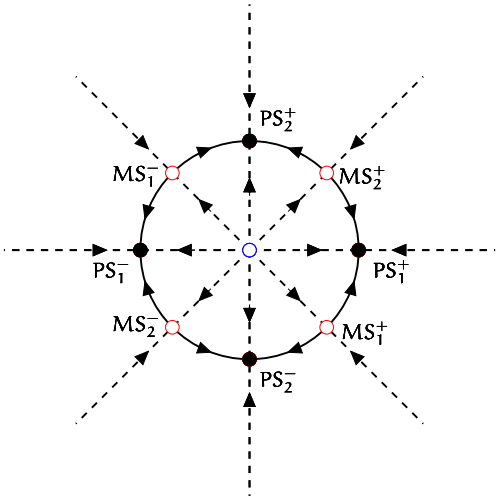

(C) The bifurcated attractor for ②. $PS_1^{\pm}$ stable, $PS_2^{\pm}$ stable and $MS_{12}^{\pm}$ saddle.

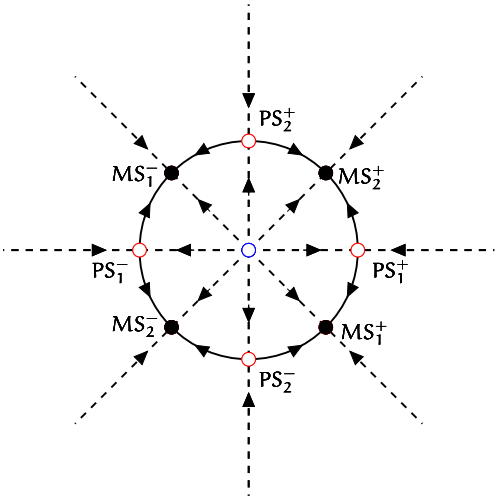

(D) The bifurcated attractor for ④. $PS_1^{\pm}$ saddle, $PS_2^{\pm}$ saddle and $MS_{12}^{\pm}$ stable.

Fig. 12. The schematic sketch of the phase portraits in the x_1–x_2 plane which display a Type-I transition behavior on $\beta_1 > 0$, $\beta_2 > 0$ where all the orbits approach a local S^1 attractor. The attractor has either 4 or 8 singular points half of which are stable nodes and the rest are saddles. The solid circles indicate stable singular points, the unfilled red circles indicate saddles and the unfilled blue circles indicate unstable nodes.

Theorem 3.3. *We consider the case that there exists a bilinear operator $\mathcal{G}_2(u, v)$ for which the nonlinear term is $\mathcal{G}(u) = \mathcal{G}_2(u, u)$ and energy preserving, that is it satisfies*

$$\langle \mathcal{G}_2(u, v), w\rangle = -\langle \mathcal{G}_2(u, w), v\rangle, \tag{31}$$

for all admissible u, v, w. Moreover we assume that the linear operator is self adjoint so that it is possible to choose the adjoint eigenmodes as

$$f_k^* = f_k, \qquad \forall k \geq 1.$$

In this case we have,

$$a > 0, \qquad d > 0, \qquad -(b + c) < 2\sqrt{ad}, \tag{32}$$

*and by Theorem 3.2, **Statement 1** holds. That is the system has an S^1 attractor bifurcation on $\lambda > \lambda_c$.*

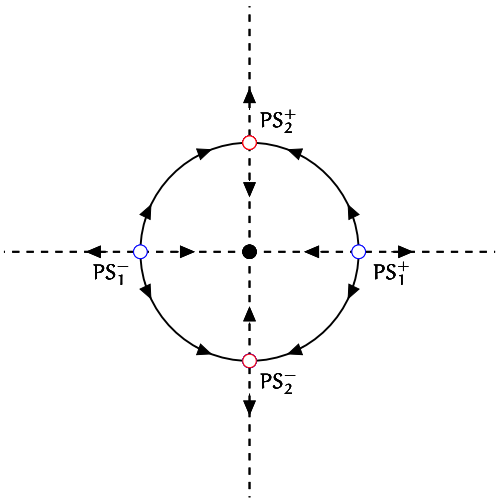

(A) The bifurcated repeller for (66). $PS_1^{\pm}$ unstable, $PS_2^{\pm}$ saddle and $MS_{12}^{\pm}$ does not exist.

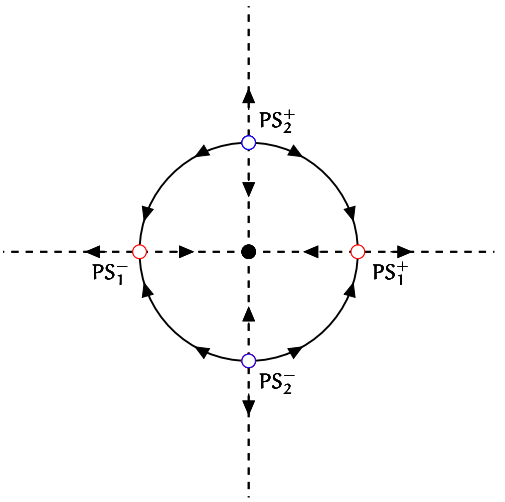

(B) The bifurcated repeller for (67). $PS_1^{\pm}$ saddle, $PS_2^{\pm}$ unstable and $MS_{12}^{\pm}$ does not exist.

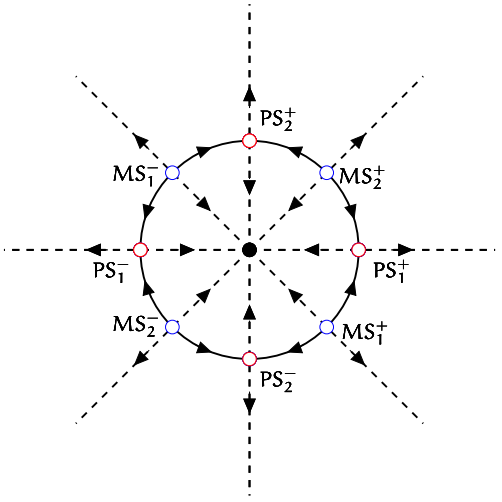

(C) The bifurcated repeller for (64). $PS_1^{\pm}$ saddle, $PS_2^{\pm}$ saddle and $MS_{12}^{\pm}$ unstable.

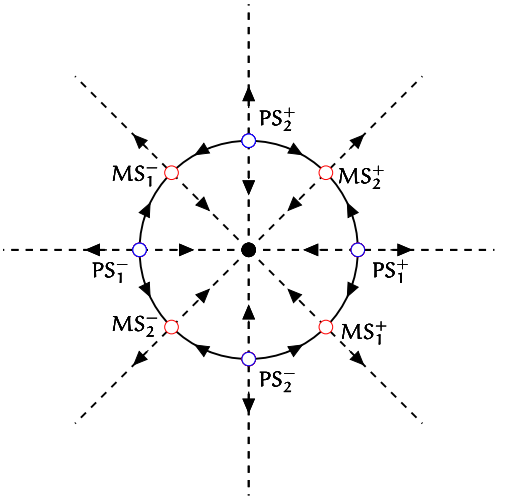

(D) The bifurcated repeller for (68). $PS_1^{\pm}$ unstable, $PS_2^{\pm}$ unstable and $MS_{12}^{\pm}$ saddle.

Fig. 13. The schematic sketch of the phase portraits in the x_1–x_2 plane which display a Type-II transition behavior accompanied by a S^1 repeller bifurcation on $\beta_1 < 0$, $\beta_2 < 0$. The repeller has either 4 or 8 singular points half of which are unstable nodes and the rest are saddles. The solid circles indicate stable singular points, the unfilled red circles indicate saddles and the unfilled blue circles indicate unstable nodes.

Proof. We normalize the eigenvectors so that

$$\langle \mathcal{M} f_i, f_j^* \rangle = \delta_{ij},$$

where δ_{ij} is the Kronecker's delta.

Recalling the definition of (19), the assumption (31) reads as

$$g_2(i,j,k) = -g_2(i,k,j), \qquad \forall i,j,k \in \mathbb{N}. \tag{33}$$

A natural consequence is

$$g_2(i,j,j) = 0, \qquad \forall i,j \in \mathbb{N}. \tag{34}$$

Hence for all $k \in \mathbb{N}$,

$$g_2^s(1,k,1) = g_2(1,k,1) + g_2(k,1,1) = g_2(1,k,1) = -g_2(1,1,k).$$

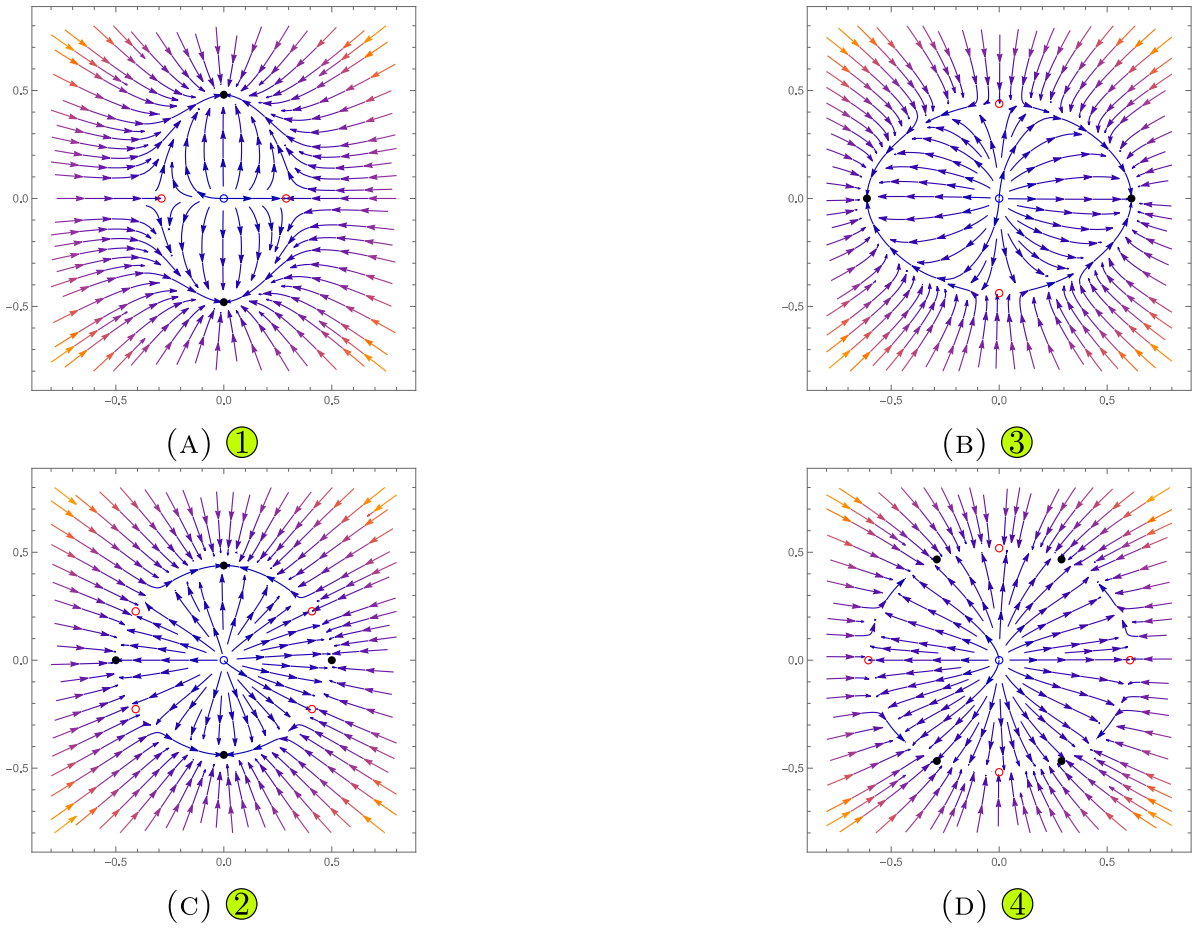

Fig. 14. The numerical simulations of the phase portraits in the x_1–x_2 plane which display a Type-I transition behavior as shown in Fig. 12.

By (26) and since the nonlinear term is bilinear, we have $g_3 \equiv 0$ and,

$$a = \sum_{k=3}^{\infty} \frac{1}{\beta_k} g_2(1,1,k) g_2^s(1,k,1) = -\sum_{k=3}^{\infty} \frac{1}{\beta_k} g_2(1,1,k)^2.$$

By (7) and by the self-adjointness of the linear operator $\beta_k = \mathrm{Re}\,\beta_k < 0$ for all $k \geq 3$. As a result, we have

$$a > 0.$$

By a similar argument, it follows that

$$d = -\sum_{k=3}^{\infty} \frac{1}{\beta_k} g_2(2,2,k)^2 > 0.$$

Since $g_3 = 0$, by (26),

$$b = \sum_{k=3}^{\infty} \frac{1}{\beta_k} \left(g_2^s(1,2,k) g_2^s(2,k,1) + g_2(2,2,k) g_2^s(1,k,1) \right),$$

$$c = \sum_{k=3}^{\infty} \frac{1}{\beta_k} \left(g_2^s(1,2,k) g_2^s(1,k,2) + g_2(1,1,k) g_2^s(2,k,2) \right).$$

Using (33), (34) and after some algebraic manipulations

$$-(b+c) = \alpha + \sum_{k=3}^{\infty} \frac{2}{\beta_k} g_2(2,2,k) g_2(1,1,k), \tag{35}$$

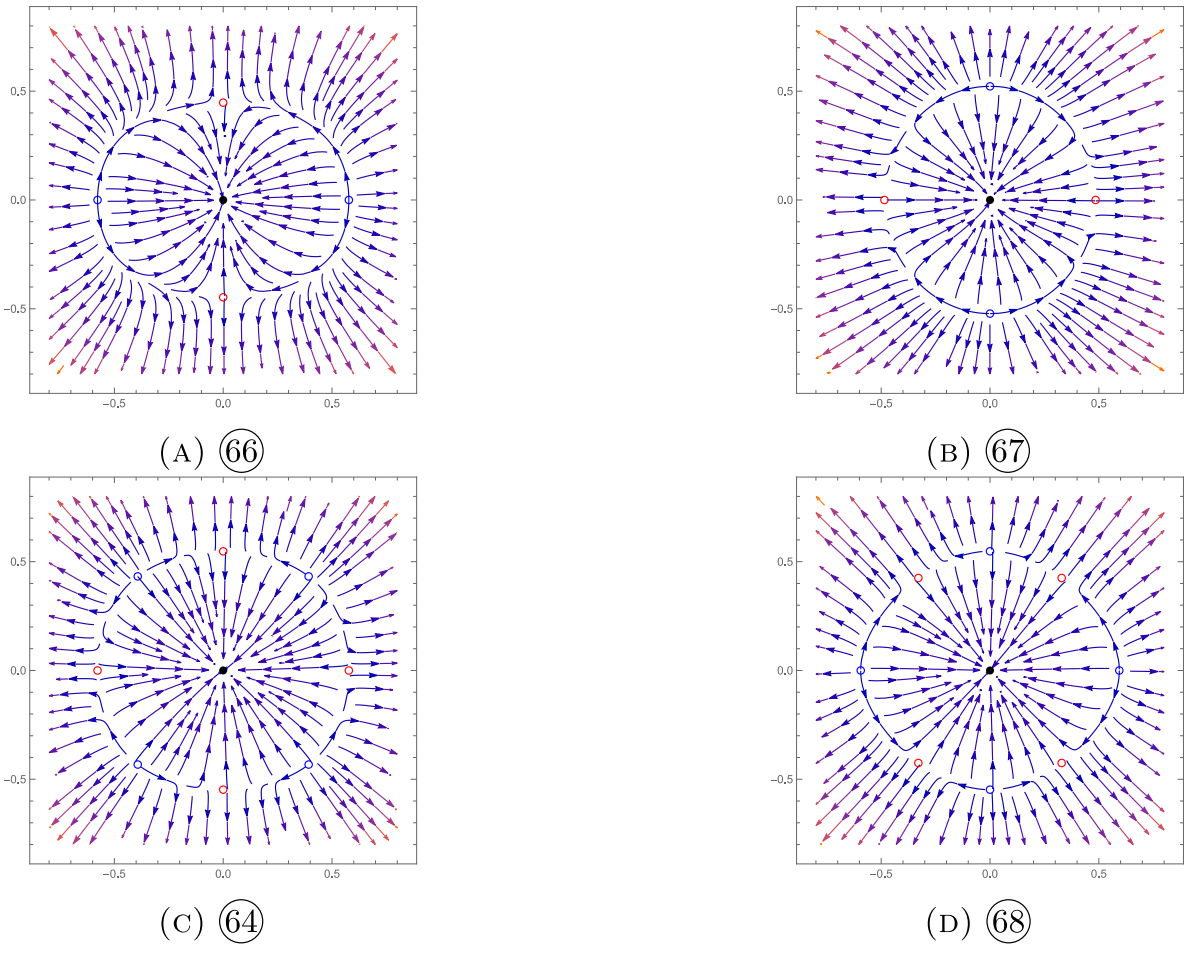

Fig. 15. The numerical simulations of the phase portraits in the x_1–x_2 plane which display a Type-II transition behavior as shown in Fig. 13.

where

$$\alpha = \sum_{k=3}^{\infty} \frac{1}{\beta_k} \left[g_2(1,k,2) + g_2(2,k,1) \right]^2 < 0,$$

since $\beta_k < 0$ for all $k \geq 3$.

Using Cauchy–Schwarz inequality gives

$$\sum_{k=3}^{\infty} \frac{2}{\beta_k} \left(g_2(2,2,k) g_2(1,1,k) \right) \leq 2 \left(-\sum_{k=3}^{\infty} \frac{1}{\beta_k} g_2(1,1,k)^2 \right)^{1/2} \left(-\sum_{k=3}^{\infty} \frac{1}{\beta_k} g_2(2,2,k)^2 \right)^{1/2}. \tag{36}$$

Combining (35) and (36) yields

$$-(b+c) \leq 2\sqrt{ad} + \alpha < 2\sqrt{ad}, \tag{37}$$

which finishes the proof.

4. Application to the 2D Rayleigh-Bénard convection

In this section, to illustrate the applicability of our theoretical results, we consider the 2D Rayleigh–Bénard problem

$$\begin{aligned} \frac{\partial \mathbf{u}}{\partial t} + \mathbf{u} \cdot \nabla \mathbf{u} &= Pr(-\nabla p + \Delta \mathbf{u}) - \mathbf{k}\sqrt{R}\sqrt{Pr}\theta, \\ \frac{\partial \theta}{\partial t} + \mathbf{u} \cdot \nabla \theta &= \sqrt{R}\sqrt{Pr}\,\Delta\theta, \end{aligned} \tag{38}$$

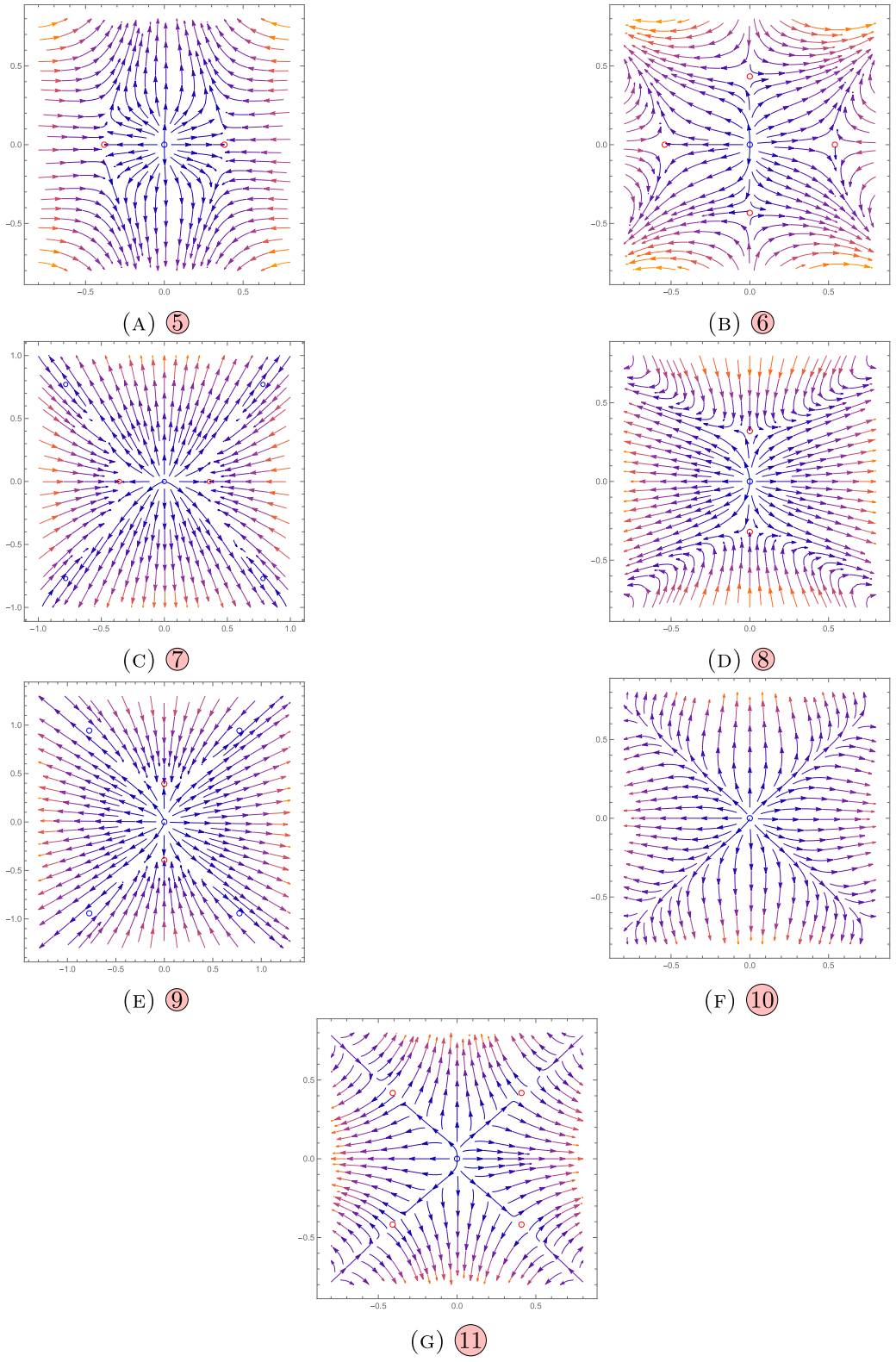

Fig. 16. The numerical simulations of the phase portraits in the x_1–x_2 plane which display a Type-II transition behavior on $\beta_1 > 0$, $\beta_2 > 0$ where the orbits leave the neighborhood of the origin.

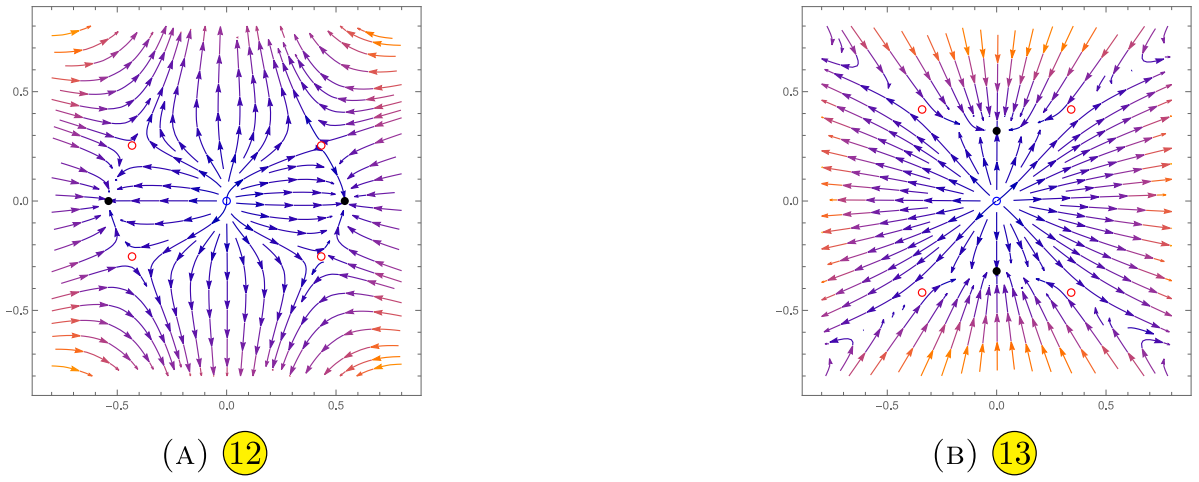

Fig. 17. The numerical simulations of the phase portraits in the x_1–x_2 plane which display a Type-III transition behavior on $\beta_1 > 0$, $\beta_2 > 0$ where the local neighborhood is separated into two disjoint regions where in one region the orbits approach a local minimal attractor while the orbits leave the local neighborhood in the other region.

posed in a rectangular box

$$(x, z) \in \Omega = (0, L) \times (0, 1).$$

In (38) $\mathbf{u} = (u, w)$ is the velocity field, θ is the temperature field and p is the pressure field. These fields are perturbations around a basic motionless state with a linear temperature field profile. Also R is the Rayleigh number which is the control parameter and Pr is the Prandtl number which depends on the physical structure of the fluid considered. Finally $\mathbf{k}$ represents the unit vector in the z-direction.

The dynamic transitions of this problem has been well studied in different settings and from different perspectives: attractor bifurcation phenomena [14,19], pattern formations in three dimensions [20], transitions in two dimensions with no-slip boundary conditions [21], with internal heating and varying gravity [22], with vertical magnetic field [16,23]. Here our goal is to show that this specific problem can be dealt with the tools we have provided in the previous sections.

We consider the problem (38) with the so called "free-slip" boundary conditions

$$\begin{aligned} &u = w_x = 0, \qquad \text{at } x = 0, L, \\ &u_z = w = 0, \qquad \text{at } z = 0, 1. \end{aligned} \tag{39}$$

We define the stream function ψ related to the velocity as $\psi_x = -w$, $\psi_z = u$. In terms of the stream function ψ, the problem (38) can be written as follows

$$\begin{aligned} &\frac{\partial \Delta\psi}{\partial t} + J(\Delta\psi, \psi) = Pr\,\Delta^2\psi - \sqrt{R}\sqrt{P_r}\theta_x, \\ &\frac{\partial \theta}{\partial t} + J(\theta, \psi) = -\sqrt{R}\sqrt{P_r}\psi_x + \Delta\theta. \end{aligned} \tag{40}$$

Here $J(f, g) = f_x g_z - f_z g_x$ is the Jacobian determinant.

The boundary conditions (39) are now as follows

$$\begin{aligned} &\psi(0, z) = \psi(L, z) = \frac{\partial^2}{\partial x^2}\psi(0, z) = \frac{\partial^2}{\partial x^2}\psi(L, z) = 0, \\ &\frac{\partial}{\partial x}\theta(0, z) = \frac{\partial}{\partial x}\theta(L, z) = 0, \\ &\psi(x, 0) = \psi(x, 1) = \frac{\partial^2}{\partial z^2}\psi(x, 0) = \frac{\partial^2}{\partial z^2}\psi(x, 1) = 0, \\ &\theta(x, 0) = \theta(x, 1) = 0. \end{aligned} \tag{41}$$

The problem can be put into the functional setting (5) by defining

$$\mathcal{M}\left(\begin{bmatrix}\psi \\ \theta\end{bmatrix}\right) = \begin{bmatrix}\Delta\psi \\ \theta\end{bmatrix}, \qquad \mathcal{N}\left(\begin{bmatrix}\psi \\ \theta\end{bmatrix}\right) = \begin{bmatrix}Pr\,\Delta^2\psi - \sqrt{R}\sqrt{P_r}\theta_x \\ -\sqrt{R}\sqrt{P_r}\psi_x + \Delta\theta\end{bmatrix},$$

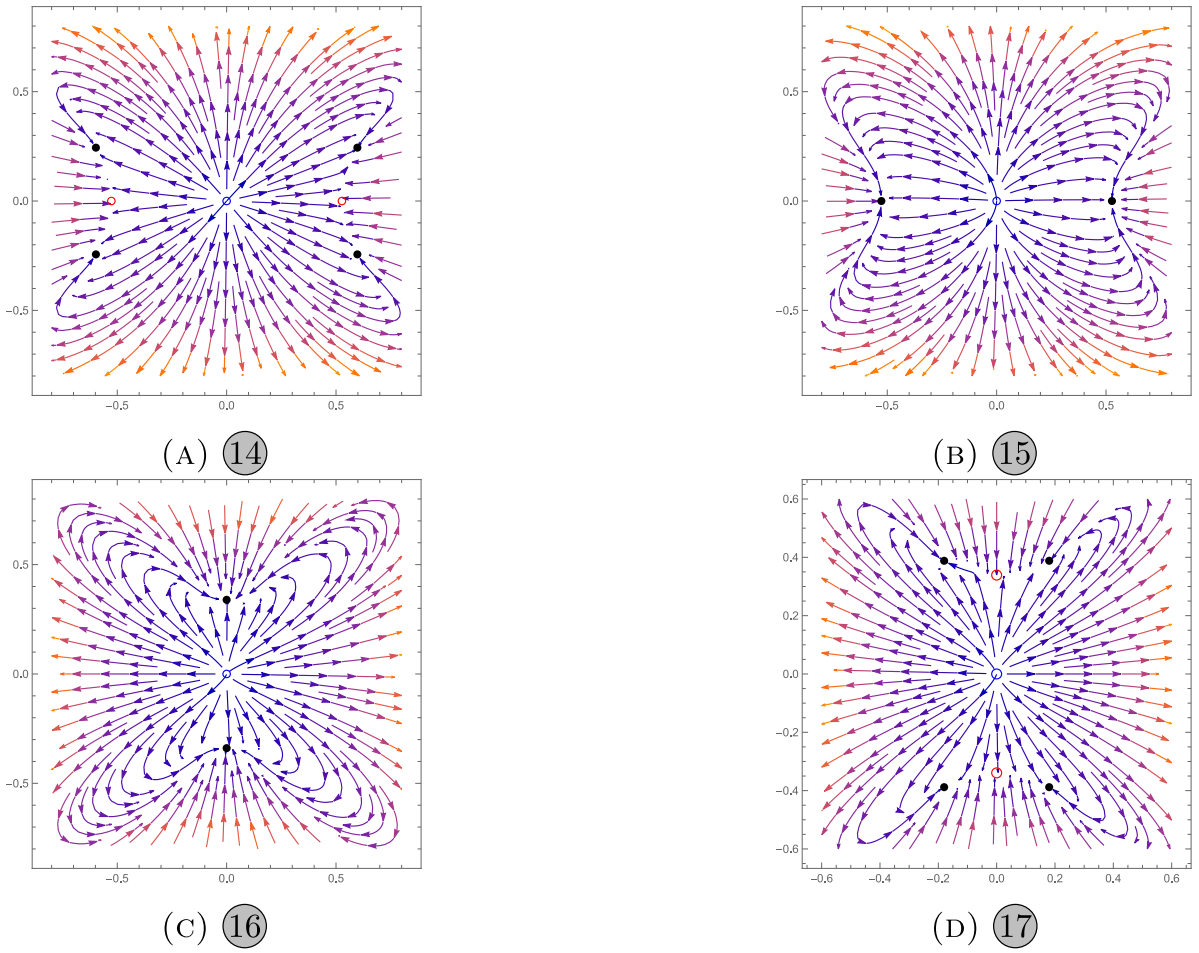

Fig. 18. The numerical simulations of the phase portraits in the x_1–x_2 plane on $\beta_1 > 0$, $\beta_2 > 0$ where the transition type is ambiguous. The local neighborhood of the origin is attracted to nearby points but the orbits leave the small neighborhood of the origin where the transition analysis is valid.

and

$$\mathcal{G}\left(\begin{bmatrix}\psi\\ \theta\end{bmatrix}\right) = \begin{bmatrix}J(\psi, \Delta\psi)\\ J(\psi,\theta)\end{bmatrix}.$$

We also define bilinear operator

$$\mathcal{G}_2\left(\begin{bmatrix}\psi_1\\ \theta_1\end{bmatrix}, \begin{bmatrix}\psi_2\\ \theta_2\end{bmatrix}\right) = \begin{bmatrix}-J(\Delta\psi_1, \psi_2)\\ J(\psi_1,\theta_2)\end{bmatrix}.$$

As discussed in Remark 2.1, the bilinear operator can be chosen in infinitely many different ways. The choice above satisfies the energy preserving condition (31) as will be shown later in (45).

The boundary conditions (41) dictate the following Fourier basis for the problem.

$$e_{m,n,1} = \begin{bmatrix}\sin\left(\frac{m\pi x}{L}\right)\sin(n\pi z)\\ 0\end{bmatrix}, \quad e_{m,n,2} = \begin{bmatrix}0\\ \cos\left(\frac{m\pi x}{L}\right)\sin(n\pi z)\end{bmatrix}. \tag{42}$$

With this basis we can express the eigenmodes of (6) by

$$c_{m,n,j}e_{m,n,1} + e_{m,n,2}, \qquad j = 1, 2, \tag{43}$$

where the coefficient is

$$c_{m,n,j} = -\frac{\gamma_{mn}^2 + \tilde{\beta}_{m,n,j}}{\sqrt{R}\sqrt{P_r}\alpha_m}, \qquad j = 1, 2.$$

Here

$$\alpha_m = m\pi/L, \qquad \gamma_{mn}^2 = \alpha_m^2 + (n\pi)^2,$$

are the horizontal and full wave numbers respectively and

$$\tilde{\beta}_{m,n,j}, \qquad j = 1, 2,$$

are the two real eigenvalues corresponding to the same wave index (m, n) with

$$\tilde{\beta}_{m,n,1} > \tilde{\beta}_{m,n,2}.$$

We then order the eigenvalues $\tilde{\beta}_{m,n,j}$ (which are all real thanks to the self-adjointness of the problem) by non-increasing values as

$$\{\beta_k : k \in \mathbb{N}\},$$

and denote the corresponding eigenmodes in (43) as

$$\{f_k : k \in \mathbb{N}\}.$$

The critical Rayleigh number (see [24]) is given by

$$R_c = \min_{m \geq 1} \frac{\left(\alpha_m^2 + \pi^2\right)^3}{\alpha_m^2}. \tag{44}$$

We note that the critical vertical index $n_0 = 1$ and the critical horizontal index depends only on the aspect ratio L of the domain and is chosen by the critical Rayleigh number (44). In Fig. 2 the selection of the critical horizontal index m_0 is shown.

At the critical aspect ratios L, a multiplicity two transition occurs with two critical eigenfunctions

$$f_1 = c_{m_0,1,1} e_{m_0,1,1} + e_{m_0,1,2},$$
$$f_2 = c_{m_0+1,1,1} e_{m_0+1,1,1} + e_{m_0+1,1,2}.$$

These aspect ratios can be seen in Fig. 2 as the L coordinate of the intersection of two marginal stability curves. The first 5 marginal stability curves intersect at the following critical aspect ratios: 2.026, 3.479, 4.910, 6.333, 7.753 with critical Rayleigh numbers 769.234, 694.282, 675.836, 668.492, 664.827. The critical Rayleigh numbers approach to the limit 657.511 as $m_0 \to \infty$. We will investigate the transition near these critical aspect ratios.

All the assumptions of our main theory are automatically satisfied with these selection of critical eigenmodes, hence our general results follow as a corollary.

(1) Near a critical aspect ratio, the PES condition (7) holds.
(2) The assumptions (13)–(16) are satisfied since at the critical aspect ratios two modes with consecutive horizontal wave indices m_0 and $m_0 + 1$ and identical vertical wave index $n_0 = 1$ become critical.
(3) The assumption (18) is valid which is a simple consequence of integrals of trigonometric functions.
(4) Moreover, the assumptions of Theorem 3.3 also hold true. The nonlinearity is bilinear that is $\mathcal{G}(u) = \mathcal{G}_2(u, u)$. Moreover the bilinear operator is energy preserving, see (31), i.e.

$$\left\langle \mathcal{G}_2\left(\begin{bmatrix}\psi_1\\ \theta_1\end{bmatrix}, \begin{bmatrix}\psi_2\\ \theta_2\end{bmatrix}\right), \begin{bmatrix}\psi_3\\ \theta_3\end{bmatrix}\right\rangle = -\left\langle \mathcal{G}_2\left(\begin{bmatrix}\psi_1\\ \theta_1\end{bmatrix}, \begin{bmatrix}\psi_3\\ \theta_3\end{bmatrix}\right), \begin{bmatrix}\psi_2\\ \theta_2\end{bmatrix}\right\rangle, \tag{45}$$

is satisfied since

$$\int_\Omega J(\Delta\psi_1, \psi_2)\psi_3 dV = -\int_\Omega J(\Delta\psi_1, \psi_3)\psi_2 dV,$$
$$\int_\Omega J(\psi_1, \theta_2)\theta_3 dV = -\int_\Omega J(\psi_1, \theta_3)\theta_2 dV,$$

due to the fact $\int_\Omega J(f, g)h dV = -\int_\Omega J(f, h)g dV$ for all admissible functions f, g, h satisfying the boundary conditions. This can be easily verified by a simple application of integration by parts.

By using the framework given in the previous sections, we obtain the following conclusions.

(1) The system near a critical aspect ratio and near the critical Rayleigh number are governed by the reduced system (25). Since the assumptions of Theorem 3.3 are satisfied, the coefficients of the reduced system satisfy $a > 0$, $d > 0$ and $-(b+c) < 2\sqrt{ad}$. Using the formulas (26), the coefficients a, d at $R = R_c$ are given by

$$a = \frac{\Pr \alpha_{m_0}^2}{L(\Pr -1)^2\,(\Pr +1-|\Pr -1|)\left(\alpha_{m_0}^2+\pi^2\right)},$$

$$d = \frac{\Pr \alpha_{m_0+1}^2}{L(\Pr -1)^2\,(\Pr +1-|\Pr -1|)\left(\alpha_{m_0+1}^2+\pi^2\right)}.$$

The coefficients b, c are also computable but their expressions are long and we omit their expressions in this discussion.

(2) Fig. 3 shows the computed values of the coefficients of the reduced system for the case $m_0 = 1$ with the aspect ratio of the domain set as $L = 2.026$ in various Prandtl number ranges. These figures indicate that a, b, d are positive for all Pr but c and $M_3 = ad - bc$ change sign when Pr is small. These values of reduced system coefficients correspond to a transition scenario given by Fig. 4. Namely depending on the values of the critical eigenvalues $\beta_1 > 0$ and $\beta_2 > 0$, the system exhibits a continuous transition and an S^1 attractor bifurcation with one of the phase portraits ①, ②, ③ and ④ shown schematically in Fig. 12 and also numerically in Fig. 14. We obtain similar results for other values of m_0.

5. Proofs

In this section, we present the proofs of our main results. We start with the reduction procedure of the main Eqs. (5) onto the center manifold. Next we analyze the reduced system and determine the steady states and their stabilities.

5.1. The reduction procedure

Here we will carry out a reduction procedure of the main Eq. (5) to a system of ODE's.
The PES condition separates the phase space X into a center space X_c and a stable subspace X_s as follows

$$X_c = \operatorname{span}\{f_1, f_2\}, \qquad X_s = \overline{\operatorname{span}\left\{f_j : j \geq 3\right\}}.$$

We consider the center part of the solution as

$$u_c(t) = x_1(t)f_1 + x_2(t)f_2 \in X_c. \tag{46}$$

We then restrict the solution to the main Eq. (5) on the center manifold $\widetilde{\Phi} \in H_s$ by writing

$$u = u_c + \widetilde{\Phi}, \tag{47}$$

where the center manifold

$$\widetilde{\Phi} = \widetilde{\Phi}(u_c)$$

is a function of the center part u_c of the solution. Then we take projection of the resulting equation on to the center space spanned by f_1, f_2.

$$\left\langle \mathcal{M}\frac{d(u_c+\widetilde{\Phi})}{dt}, f_j^* \right\rangle = \langle \mathcal{N}(u_c+\widetilde{\Phi}) + \mathcal{G}(u_c+\widetilde{\Phi}), f_j^* \rangle, \qquad j = 1, 2, \tag{48}$$

where f_j^* are the adjoint critical eigenmodes. By the adjoincy condition (8) and the orthogonality condition (9), we get

$$\frac{dx_j}{dt} = \beta_j x_j + \frac{1}{\langle \mathcal{M}f_j, f_j^* \rangle}\langle \mathcal{G}(u_c+\widetilde{\Phi}), f_j^* \rangle, \qquad j = 1, 2. \tag{49}$$

5.1.1. Quadratic approximation of the center manifold

We now write the center manifold as

$$\widetilde{\Phi} = \Phi + O(3),$$

where Φ is the quadratic approximation of $\widetilde{\Phi}$ and $O(3)$ represents higher order terms in (x_1, x_2).

By the approximation theorem for the center manifold, see [3], in the case of real critical eigenvalues (7), we have the formula

$$-\Pi_s \mathcal{N}\Phi = \mathcal{G}_2(u_c, u_c), \tag{50}$$

where Π_s is the projection operator onto the stable space X_s.

Also by plugging in the expansion

$$\Phi = \sum_{k=3}^{\infty} \hat{\Phi}_k f_k,$$

into (50), taking inner product with f_k^*, We obtain from (50), the spectral components of the center manifold as

$$\hat{\Phi}_k = \frac{-1}{\beta_k \langle \mathcal{M} f_k, f_k^* \rangle} \langle \mathcal{G}_2(u_c, u_c), f_k^* \rangle = x_1^2 \Phi_{20,k} + x_1 x_2 \Phi_{11,k} + x_2^2 \Phi_{02,k}, \tag{51}$$

where by using the notation in (19), we define for $k \geq 3$,

$$\begin{aligned} \Phi_{20,k} &= -\frac{1}{\beta_k} g_2(1,1,k), \\ \Phi_{11,k} &= -\frac{1}{\beta_k} g_2^s(1,2,k), \\ \Phi_{02,k} &= -\frac{1}{\beta_k} g_2(2,2,k). \end{aligned} \tag{52}$$

The formulas (52) mean that to the lowest order the center manifold is determined by the bilinear interactions of the critical modes with higher order modes.

5.1.2. Approximation of the reduced equations

The approximation of the reduced Eq. (49) can be written as

$$\frac{dx_j}{dt} = \beta_j x_j + Q_j(x_1, x_2) + C_j(x_1, x_2) + o(3), \qquad j = 1, 2, \tag{53}$$

where Q_j, C_j denotes the quadratic and cubic terms respectively.

Using (49)–(52), the quadratic Q_j and cubic C_j terms are given as follows for $j = 1, 2$

$$\begin{aligned} Q_j(x_1, x_2) &= Q_{j1} x_1^2 + Q_{j2} x_1 x_2 + Q_{j3} x_2^2, \\ C_j(x_1, x_2) &= C_{j1} x_1^3 + C_{j2} x_1^2 x_2 + C_{j3} x_1 x_2^2 + C_{j4} x_2^3, \end{aligned} \tag{54}$$

where for $j = 1, 2$,

$$Q_{j1} = g_2(1,1,j), \qquad Q_{j2} = g_2^s(1,2,j), \qquad Q_{j3} = g_2(2,2,j), \tag{55}$$

and

$$\begin{aligned} C_{j1} &= g_3(1,1,1,j) + \sum_{k=3}^{\infty} \Phi_{20,k} g_2^s(1,k,j), \\ C_{j2} &= g_3^s(1,1,2,j) + \sum_{k=3}^{\infty} \left(\Phi_{11,k} g_2^s(1,k,j) + \Phi_{20,k} g_2^s(2,k,j) \right), \\ C_{j3} &= g_3^s(1,2,2,j) + \sum_{k=3}^{\infty} \left(\Phi_{11,k} g_2^s(2,k,j) + \Phi_{02,k} g_2^s(1,k,j) \right), \\ C_{j4} &= g_3(2,2,2,j) + \sum_{k=3}^{\infty} \Phi_{02,k} g_2^s(2,k,j). \end{aligned} \tag{56}$$

5.1.3. Quadratic terms of the reduced equations

The coefficients of the quadratic terms of the reduced equations given by (55) all vanish due to (21). We recall that the reason for the vanishing of the quadratic terms of the reduced equations are due to the identical vertical wave index selection (n_0) of the critical modes.

5.1.4. Cubic terms of the reduced equations

Now we will show that the cubic terms of the first equation of the reduced system is free from $x_1^2 x_2$, x_2^3 and the cubic terms of the second equation are free from x_1^3, $x_1 x_2^2$. The provided proof shows that this is simply a consequence of the assumption of consecutive critical horizontal wave index selection: m_0, $m_0 + 1$.

Lemma 5.1. *The following cubic terms of the reduced equation vanish.*

$$C_{12} = C_{14} = C_{21} = C_{23} = 0.$$

Proof. We first recall that

$$C_{12} = g_3^s(1,1,2,1) + \sum_{k=3}^{\infty} \left(\Phi_{11,k} g_2^s(1,k,1) + \Phi_{20,k} g_2^s(2,k,1) \right).$$

By (24), $g_3^s(1,1,2,1) = 0$ and so there is no contribution to C_{12} from the trilinear critical mode interactions.

Now let

$$V_1 = \bigoplus_{(m,n)\in\{0,2m_0\}\times\{0,2n_0\}} H_{m,n},$$

$$V_2 = \bigoplus_{(m,n)\in\{\pm(1+2m_0),\pm 1\}\times\{0,2n_0\}} H_{m,n},$$

where $\bigoplus$ denotes the direct sum of subspaces and $H_{m,n}$ are the subspaces given by (12). Then by (18),

$$g_2^s(1,k,1) \neq 0 \iff f_k \in V_1,$$

and

$$g_2^s(1,2,k) \neq 0 \iff f_k \in V_2.$$

Notice that by (52), the latter condition implies

$$\Phi_{11,k} \neq 0 \iff f_k \in V_2.$$

Since $V_1 \cap V_2 = \{0\}$, there is no k for which $f_k \in V_1 \cap V_2$ and as a result,

$$\Phi_{11,k} g_2^s(1,k,1) = 0, \qquad \forall k \geq 3.$$

Similarly, one can show that

$$\Phi_{20,k} g_2^s(2,k,1) = 0, \qquad \forall k \geq 3.$$

That finishes the proof that $C_{12} = 0$.

The remaining proofs $C_{14} = C_{21} = C_{23} = 0$ are identical and left to the reader.

5.2. The existence and stability of the bifurcated steady state solutions

In this subsection we analyze the dynamical behavior of the reduced Eqs. (25). For this we consider the truncated system of (25) where $O(4)$ terms are omitted.

$$\begin{aligned} \frac{dx_1}{dt} &= \beta_1(\lambda)x_1 - x_1(ax_1^2 + bx_2^2), \\ \frac{dx_2}{dt} &= \beta_2(\lambda)x_2 - x_2(cx_1^2 + dx_2^2). \end{aligned} \tag{57}$$

The fixed points of (57) are as follows:

(1) The trivial fixed point $(0,0)$ which always exist,

(2) The four possible "pure" fixed points

$$\left(\pm\sqrt{\frac{\beta_1}{a}}, 0 \right), \qquad \left(0, \pm\sqrt{\frac{\beta_2}{d}} \right).$$

(3) The four possible "mixed" fixed points

$$\left(\pm\sqrt{\frac{M_1}{M_3}}, \sqrt{\frac{M_2}{M_3}} \right), \qquad \left(\pm\sqrt{\frac{M_1}{M_3}}, -\sqrt{\frac{M_2}{M_3}} \right),$$

which are found as the solution of

$$\begin{aligned} \beta_1 &= ax_1^2 + bx_2^2, \\ \beta_2 &= cx_1^2 + dx_2^2, \end{aligned}$$

where M_1, M_2 and M_3 are given by (27).

Next we investigate the stabilities of these fixed points. The Jacobian matrix of the right hand side of (57) is given by

$$J(x_1,x_2) = \begin{bmatrix} \beta_1 - 3ax_1^2 - bx_2^2 & -2bx_1x_2 \\ -2cx_1x_2 & \beta_2 - cx_1^2 - 3dx_2^2 \end{bmatrix}.$$

The eigenvalues λ_1, λ_2 of the Jacobian matrix evaluated at the fixed points are as follows.

(1) For the trivial fixed point $(0, 0)$,

$$\lambda_1 = \beta_1, \qquad \lambda_2 = \beta_2.$$

(2) For the pure fixed points $\left(\pm\sqrt{\frac{\beta_1}{a}}, 0\right)$,

$$\lambda_1 = -2\beta_1, \qquad \lambda_2 = \frac{M_2}{a}.$$

(3) For the pure fixed points $\left(0, \pm\sqrt{\frac{\beta_2}{d}}\right)$,

$$\lambda_1 = \frac{M_1}{d}, \qquad \lambda_2 = -2\beta_2.$$

(4) For the mixed fixed points, the eigenvalues satisfy

$$\lambda^2 - \tau\lambda + \delta = 0,$$

where

$$\tau = -2\frac{aM_1 + dM_2}{M_3}, \qquad \delta = 4\frac{M_1M_2}{M_3}.$$

Now the analysis of the signs of the eigenvalues give the stabilities of the corresponding fixed points which yield Table 1.

6. Summary and discussion

(1) Dynamic transition analysis has been an active research area in the last decade, with numerous studies using this approach to analyze specific problems in nonlinear systems [3]. The aim of this work is to classify the dynamic transitions of a broad class of problems that satisfy certain assumptions. The main novelty and contribution of this work is the classification of dynamic transitions that arise in nonlinear systems with two critical eigenvalues whose eigenmodes have wave indices (m_0, n_0) and (m_0+1, n_0). This assumption is a natural one for many nonlinear dynamic transition problems, including the Rayleigh–Bénard convection problem which we study as an application of our main results.

(2) The main contribution of this paper is to provide a comprehensive analysis of the dynamic transitions of a wide range of nonlinear systems of PDEs that satisfy certain assumptions near the criticality. The paper presents a reduced system of ODEs that describes all possible dynamic transition scenarios, and carefully analyzes these scenarios. We believe that this framework will be of great value to researchers who are interested in identifying the dynamic transitions of specific problems in various fields of study.
We also investigate a special case, where the linear operator is self-adjoint, the nonlinear term is bilinear and the bilinearity can be chosen as energy-preserving which are the typical assumptions for the 2D Navier–Stokes equations. Under these conditions we show that the system exhibits a continuous type transition with a S^1 attractor bifurcation at critical aspect ratios where two eigenvalues become unstable simultaneously.

(3) To illustrate the applicability of the general framework obtained, we consider an application of our main results to the 2D Rayleigh–Bénard convection problem with free-slip boundary conditions in a rectangular domain. We show that this problem displays an S^1 attractor bifurcation which is a direct consequence of our results.

(4) There are several future questions/research directions that have arised during this study some of which are as follows.

(a) While our main assumption in this work is the existence of two eigenmodes with two separate wave indices, one of which is consecutive and the other identical, there are other wave index selections that occur naturally in dynamic transition problems. We plan to extend our methodology to cover these other cases.
(b) In our analysis of the reduced system, we encountered several phase portraits where the transition type is ambiguous. We believe that considering higher-order approximations of the reduced system could resolve this ambiguity.
(c) This study can be extended to cover multiplicity three and higher transitions, as in [11].
(d) An important and interesting question is to carry out the analysis of this paper in cases where the first two critical eigenvalues are non-real, leading to a double Hopf bifurcation. This has been observed by other researchers [25–28].
(e) The transitions from non-constant steady states and geometries other than the rectangular domains studied in this manuscript are also interesting research directions.

7. Tables and figures

To enhance the readability of the paper, we collect various tables and figures in this section that are referred inside this manuscript.

Here, we show in Table 2, the existence and stability of steady states in all the possible phase portraits of (5) near $(u, \lambda) = (0, \lambda_c)$. In Figs. 4–11 we show all the possible transition scenarios.

In Figs. 4–11 the dashed line (– –) represents M_1, the dash-dotted (· –) line represents M_2 and the dotted line (· · ·) represents $aM_1 + dM_2$ where M_1, M_2 are defined in (27) and a, d are defined in (26).

The multiplicity two transitions when both eigenvalues are positive are shown schematically in Figs. 12–13 and numerically in Figs. 14–18.

CRediT authorship contribution statement

Taylan Şengül: Conceptualization, Methodology, Supervision, Writing – review & editing. **Burhan Tiryakioglu:** Conceptualization, Formal analysis, Investigation, Writing – original draft.

Declaration of competing interest

The authors declare that they have no known competing financial interests or personal relationships that could have appeared to influence the work reported in this paper.

Data availability

Data will be made available on request.

Acknowledgment

The authors would like to thank the anonymous reviewer for his/her valuable comments.

References

[1] Temam Roger. Infinite-dimensional dynamical systems in mechanics and physics. Applied mathematical sciences, vol. 68, New York: Springer; 1997,
[2] Chekroun Mickaël D, Liu Honghu, McWilliams James C, Wang Shouhong. Transitions in stochastic non-equilibrium systems: Efficient reduction and analysis. J Differential Equations 2023;346:145–204.
[3] Ma Tian, Wang Shouhong. Phase transition dynamics. Cham: Springer International Publishing; 2019.
[4] Ma Tian, Wang Shouhong. Bifurcation theory and applications. World scientific series on nonlinear science series A, vol. 53, World Scientific; 2005.
[5] Şengül Taylan. Dynamical transition theory of hexagonal pattern formations. Commun Nonlinear Sci Numer Simul 2020;91:105455.
[6] Şengül Taylan, Tiryakioglu Burhan. Dynamic transitions and bifurcations of 1D reaction–diffusion equations: The self-adjoint case. Math Methods Appl Sci 2022;45(5):2871–92.
[7] Şengül Taylan, Tiryakioglu Burhan. Dynamic transitions and bifurcations of 1D reaction-diffusion equations: The non-self-adjoint case. J Math Anal Appl 2023;523(1):127114.
[8] Jia Lan, Li Liang. Stability and dynamic transition of vegetation model for flat arid terrains. Discrete Continuous Dyn Syst - B 2021.
[9] Choi Yuncherl, Ha Taeyoung, Han Jongmin, Kim Sewoong, Lee Doo Seok. Turing instability and dynamic phase transition for the Brusselator model with multiple critical eigenvalues. Discr Contin Dyn Syst 2021;41(9):4255.
[10] Muntari Umar Faruk, Şengül Taylan. Dynamic transitions and Turing patterns of the Brusselator model. Math Methods Appl Sci 2022;45(16):9130–51.
[11] Wang Quan, Yan Dongming. On the stability and transition of the Cahn-Hilliard/Allen-Cahn system. Discrete Continuous Dyn Syst - B 2020;25(7):2607.
[12] Liu Honghu, Sengul Taylan, Wang Shouhong, Zhang Pingwen. Dynamic transitions and pattern formations for a Cahn–Hilliard model with long-range repulsive interactions. Commun Math Sci 2015;13(5):1289–315.
[13] Liu Honghu, Sengul Taylan, Wang Shouhong. Dynamic transitions for quasilinear systems and Cahn-Hilliard equation with Onsager mobility. J Math Phys 2012;53(2):023518.
[14] Ma Tian, Wang Shouhong. Dynamic bifurcation and stability in the Rayleigh-benard convection. Commun Math Sci 2004;2(2):159–83.
[15] Li Junyan, Wu Ruili. Dynamic transition analysis for activator-substrate system. J Nonlinear Math Phys 2023.
[16] Han Daozhi, Hernandez Marco, Wang Quan. Dynamical transitions of a low-dimensional model for Rayleigh–Bénard convection under a vertical magnetic field. Chaos Solitons Fractals 2018;114:370–80.
[17] Li Liang, Fan Yanlong, Han Daozhi, Wang Quan. Dynamical transition and bifurcation of hydromagnetic convection in a rotating fluid layer. Commun Nonlinear Sci Numer Simul 2022;112:106531.
[18] Pan Zhigang, Jia Lan, Mao Yiqiu, Wang Quan. Transitions and bifurcations in couple stress fluid saturated porous media using a thermal non-equilibrium model. Appl Math Comput 2022;415:126727.
[19] Ma Tian, Wang Shouhong. Attractor bifurcation theory and its applications to Rayleigh-Bénard convection. Commun Pure Appl Anal 2003;2(4):591.
[20] Sengul Taylan, Wang Shouhong. Pattern formation in Rayleigh–Bénard convection. Commun Math Sci 2013;11(1):315–43.
[21] Sengul Taylan, Shen Jie, Wang Shouhong. Pattern formations of 2D Rayleigh-Bénard convection with no-slip boundary conditions for the velocity at the critical length scales. Math Methods Appl Sci 2015;38(17):3792–806.

[22] Han Daozhi, Hernandez Marco, Wang Quan. Dynamic bifurcation and transition in the Rayleigh–Bénard convection with internal heating and varying gravity. Commun Math Sci 2019;17(1):175–92.
[23] Sengul Taylan, Wang Shouhong. Pattern formation and dynamic transition for magnetohydrodynamic convection. Commun Pure Appl Anal 2014;13(6):2609–39.
[24] Chandrasekhar Subrahmanyan. Hydrodynamic and hydromagnetic stability. The international series of monographs on physics, Clarendon Press, city=Oxford; 1961.
[25] Pan Zhigang, Wang Quan, Sengul Taylan. On the viscous instabilities and transitions of two-layer model with a layered topography. Commun Nonlinear Sci Numer Simul 2020;80:104978.
[26] Pan Zhigang, Kieu Chanh, Wang Quan. Hopf bifurcations and transitions of two-dimensional quasi-geostrophic flows. Commun Pure Appl Anal 2021;20(4):1385–412.
[27] Mao Yiqiu, Chen Zhimin, Kieu Chanh, Wang Quan. On the stability and bifurcation of the non-rotating Boussinesq equation with the Kolmogorov forcing at a low Péclet number. Commun Nonlinear Sci Numer Simul 2020;89:105322.
[28] Chekroun Mickaël D, Dijkstra Henk, Şengül Taylan, Wang Shouhong. Transitions of zonal flows in a two-layer quasi-geostrophic ocean model. Nonlinear Dynam 2022;109(3):1887–904.